

On the jet properties of the γ -ray loud active galactic nuclei

Liang Chen^{1,2}

ABSTRACT

Based on broadband spectral energy distribution (SEDs), we estimate the jet physical parameters of 1392 γ -ray-loud active galactic nuclei (AGNs), the largest sample so far. The (SED) jet power and magnetization parameter are derived for these AGNs. Out of these sources, the accretion disk luminosity of 232 sources and (extended) kinetic jet powers of 159 sources are compiled from archived papers. We find the following, (1) Flat-spectrum radio quasars (FSRQs) and BL Lacs are well separated by $\Gamma = -0.127 \log L_\gamma + 8.18$, in γ -ray luminosity versus photon index plane with a success rate of 88.6%. (2) Most FSRQs present a (SED) jet power larger than the accretion power, which suggests that the relativistic jet-launching mechanism is dominated by the Blandford-Znajek process. This result confirms previous findings. (3) There is a significant anticorrelation between jet magnetization and a ratio of the (SED) jet power to the (extended) kinetic jet power, which, for the first time, provides supporting evidence for the jet energy transportation theory: a high-magnetization jet may be more easily to transport energy to a large scale than a low-magnetization jet.

Subject headings: galaxies: active - galaxies: jets - BL Lacertae objects: general - quasars: general - radiation mechanisms: non-thermal

1. Introduction

The gravitational potential of the supermassive black hole (BH), at the center of an active galactic nucleus (AGN), is believed to be the ultimate energy source of the AGN.

¹Key Laboratory for Research in Galaxies and Cosmology, Shanghai Astronomical Observatory, Chinese Academy of Sciences, 80 Nandan Road, Shanghai 200030, China; E-mail: chenliang@shao.ac.cn

²University of Chinese Academy of Science, 19A Yuquanlu, Beijing 100049, China

An accretion disk can be formed during way of matter falling onto the BH, and the angular momentum can be lost through viscosity or turbulence (e.g., Rees 1984) or via outflow or magnetic field processes (e.g., Cao 2011; Cao & Spruit 2013). About 10% of AGNs have relative stronger radio emissions compared with their optical emissions (i.e., radio-loud AGNs¹), which are believed to host relativistic jets launched from the central accreting system (Urry & Padovani 1995; Yuan et al. 2008; Cao 2016). The jet launching can be related to the Blandford-Znajek (BZ) process (Blandford & Znajek 1977) through extracting the rotational energy of BHs and/or the Blandford-Payne (BP) process (Blandford & Payne 1982) by releasing the gravitational energy of the accretion disk. As an extreme subclass of radio-loud AGNs, blazars show broadband emissions (radio through γ -ray), rapid variability, high and variable polarization, superluminal motions, and core-dominated nonthermal continua, which are believed to be caused by a relativistic Doppler-beaming effect due to a small viewing angle between the relativistic jet and the line of sight (see, e.g., Blandford & Rees 1978; Urry & Padovani 1995; Falomo et al. 2014; Madejski & Sikora 2016). These properties provide the blazar an ideal laboratory to study AGN jet physics. Broadband spectral energy distributions (SEDs) of blazars usually show two significant bumps: one peaks at the infrared (IR) to X-ray bands, which is believed to be the synchrotron emission of energetic electrons within the jet; and the second bump peaks at the γ -ray band, which may be the inverse Compton (IC) emission of the same electron population emitting the synchrotron bump (e.g., Bloom & Marscher 1996; Sikora et al. 1994; Dermer & Schlickeiser 1993, see also the hadronic model, Mannheim (1993); Aharonian (2000)). According to the rest-frame equivalent width (EW) of the broad emission lines, blazars are classified as flat-spectrum radio quasars (FSRQs) with $EW \geq 5\text{\AA}$ and BL Lacertae objects (BL Lacs) with $EW < 5\text{\AA}$ (see Scarpa & Falomo 1997).

Indisputably, the jet property is basically important in studying jet physics, including the jet launching, energy transportation, energy transform and conversion, radiative processes, etc. Limited by spatial resolution of modern telescopes, only the very long baseline interferometry (VLBI) radio technique can resolve subparsec-scale jet (even down to several Schwarzschild radii for very near and massive BHs, e.g., M87, Doeleman et al. 2012). Superluminal motion is a common phenomenon in blazar VLBI observations, which set a strong constraint that these jets should move very fast (apparent velocity on the order of $\beta_{\text{app}} \equiv v_{\text{app}}/c \gtrsim 10$, and can reach ~ 30 for some special sources; see, e.g., Lister et al. 2013). The rapid variability at the γ -ray band can also set a lower limit of jet velocity due to the fact that these γ -ray photons are actually escaped from the emission region

¹The radio-loudness parameter, the ratio of the radio flux at 5 GHz to the optical flux at the B band, $R \equiv f_{5\text{GHz}}/f_B > 10$ for radio-loud AGNs (Kellermann et al. 1989).

by overcoming the possible absorption of soft photons through photon annihilation (e.g., Dondi & Ghisellini 1995). The jet properties at the launching and energy dissipation regions can also be constrained through broadband SED modeling (e.g., Ghisellini et al. 1998, 2014; Ghisellini & Tavecchio 2015; Chen 2017). This powerful method can offer a constraint on the main jet parameters, including, within the one-zone leptonic model, the Doppler factor (the bulk Lorentz factor sometimes), the strength of the magnetic field, the energy density of the relativistic electrons, the jet power, the energy distribution of the electrons, and the location of the emission region (e.g., Ghisellini et al. 2014; Ghisellini & Tavecchio 2015; Kang et al. 2014; Chen 2017). Benefit from a better knowledge of the high-frequency radio, millimeter, far-IR, and γ -ray continuum given by the *WMAP*, *Planck*, *WISE* and *Fermi* Large Area Telescope (LAT) satellites, Ghisellini et al. (2014) modeled the broadband SED of the largest blazar sample yet (the number of blazars reaches 217; see also Ghisellini & Tavecchio 2015) and got the jet physical parameters. Note that within the one-zone leptonic model, the estimation of the jet parameters mainly depends on the peak frequency and luminosity of the two SED bumps (see, e.g., Tavecchio et al. 1998; Chen 2017).

Since its launch on 2008 June 11, the LAT onboard the *Fermi* satellite has revolutionized our knowledge of the γ -ray AGNs above 100 MeV. A large number of AGNs are detected by *Fermi*/LAT and are compiled as the LAT Bright AGN Sample (LBAS; Abdo et al. 2009) and the First/Second/Third LAT AGN Catalogs (1LAC/2LAC/3LAC; Abdo et al. 2010; Ackermann et al. 2011, 2015). The 3LAC includes 1591 AGNs located at high Galactic latitudes ($|b| > 10^\circ$) and detected at $\gtrsim 100$ MeV with a test statistic greater than 25 between 2008 August 4 and 2012 July 31. The number of γ -ray AGNs is even beyond the previous estimation (e.g., Cao & Bai 2008). Most of these AGNs are blazars (98%) and can be obtained with radio, optical, and X-ray data. In this paper, we will investigate the AGN jet physics based on broadband SED. The Section 2 describes the sample. The Section 3 presents the method to calculate the jet parameters. The result and discussion will be given in the Section 4. Our conclusion will be drawn in the Section 5. A Λ CDM cosmology with values from the Planck results is used in our calculation; in particular, $\Omega_m = 0.32$, $\Omega_\Lambda = 0.68$, and the Hubble constant $H_0 = 67 \text{ km s}^{-1} \text{ Mpc}^{-1}$ (Planck Collaboration et al. 2014).

2. Sample

The 3LAC contains 1591 AGNs, of which 1559 are blazars (467 FSRQs, 632 BL Lacs, and 460 BCUs²). Due to the uniform all-sky exposure of the *Fermi*/LAT, these sources form

²BCU refers to the blazar candidates of uncertain type (Ackermann et al. 2015).

a γ -ray flux-limited sample. Note that since the blazars are rapidly variable, it is better to use the simultaneous multifrequency data, which seems impossible for the 3LAC, given the very large number of sources. Through collecting the multifrequency data (radio to X-ray bands) from the NASA/IPAC Extragalactic Database (NED), Fan et al. (2016) successfully obtained the broadband SED of 1392 blazars (461 FSRQs, 620 BL Lacs, and 311 BCUs). They employed a log-parabolic function, $\log(\nu F_\nu) = -P_1(\log \nu - \log \nu_p)^2 + \log(\nu_p F_{\nu_p})$, to fit the SED; therefore, the synchrotron peak frequency (ν_p), spectral curvature (P_1), and the peak flux ($\nu_p F_{\nu_p}$) are obtained. Of the total number of blazars, 999 have measured redshifts. In this paper, we will study the jet physical properties of the 1392 blazars, based on the data of Fan et al. (2016). The data regarding the γ -ray (i.e., photon index and luminosity) are compiled from Ackermann et al. (2015) and Acero et al. (2015).

3. Methods

We directly collect the peak frequency and flux of the synchrotron bump from Fan et al. (2016). For the IC bump, the observed γ -ray luminosity and photon index are used to estimate the peak luminosity and frequency. Abdo et al. (2010) collected quasi-simultaneous broadband SEDs of 48 blazars and employed a third-degree polynomial to fit the synchrotron and IC bumps. The obtained peak frequency and luminosity are found to be significantly correlated with the γ -ray photon index and γ -ray luminosity, respectively. They found a tight relation between the photon index and IC peak frequency: $\log \nu_{IC}^p = -4\Gamma + 31.6$ (see Equation 5 in Abdo et al. 2010). For the same sample, we plot γ -ray luminosity versus IC peak luminosity in Figure 1. The linear fitting shows $\log L_{IC}^p = (0.946 \pm 0.018) \log L_\gamma + (2.18 \pm 0.88)$ and the Pearson test yields the chance probability $p = 8.72 \times 10^{-39}$. Because there is not enough data to construct the IC bump for this large sample, the above two formulae are used to estimate the IC peak frequency and luminosity.

For BL Lac objects, the optical emission lines are very weak or even missed. Their γ -ray emission is believed to be synchrotron self-Compton (SSC) emission. The γ -ray emission of FSRQs, with strong optical emission lines, is believed to be emission from IC external seed photons produced (EC) from, e.g., a broad emission-line region (BLR) or dust torus. As suggested by Ghisellini et al. (2009), BL Lacs and FSRQs are neatly separated in the γ -ray photon index versus γ -ray luminosity plane (see also Abdo et al. 2009; Ackermann et al. 2015). For confirmed FSRQs and BL Lacs in the 3LAC (Ackermann et al. 2015), we plot the γ -ray photon index versus γ -ray luminosity in the Figure 2. It can be seen that FSRQs have larger γ -ray luminosity and softer γ -ray spectra (red squares, mostly in the upper right corner) compared with BL Lacs (blue squares, mostly in the lower left corner). The

physical difference between these two subclasses may be related to the different accretion model of the central BH; i.e., a standard cold accretion disk exists in FSRQs, while advection-dominated accretion flow (ADAF; Yuan & Narayan 2014) exists in BL Lacs (e.g., Wang et al. 2002; Cao 2003; Xu et al. 2009; Ghisellini et al. 2009; Sbarrato et al. 2014). Despite of the different physical origin, we choose a phenomenological criterion (a line in the γ -ray photon index versus luminosity plane) to roughly separate these two subclasses. This criterion/line should satisfy two criteria (see the Figure 2): (1) the fraction of FSRQs above the line and the fraction of BL Lacs below the line should be same, and (2) this fraction value must reach maximum. Finally, we get the criterion (the black line in the Figure 2): $\Gamma = -0.127 \log L_\gamma + 8.18$. In this case, the fraction of FSRQs above the line and the fraction of BL Lacs below the line reaches the maximum value: 88.6%. As mentioned above, 311 out of 1932 blazars are BCUs. In this paper, this criterion is employed to classify these BCUs into FSRQs or BL Lacs. In this case, the class type is labeled “UF” for BCUs classified as FSRQs and “UB” for BCUs classified as BL Lacs, while, the class types “CF” and “CB” are for these confirmed FSRQs and BL Lacs, respectively (see the class type in Table 1).

The SSC emission of FSRQs usually peaks at the X-ray band and dominates its X-ray emission (see, e.g., Kang et al. 2014; Zhang et al. 2015; Ghisellini & Tavecchio 2015). Therefore, the X-ray luminosity can be set as the upper limit of the SSC luminosity in FSRQs. Fan et al. (2016) presented X-ray luminosity at 1 keV for 275 out of 486 FSRQs and found a tight relation between X-ray and γ -ray luminosity, $L_{1\text{GeV}} = 0.91L_{1\text{keV}} + 5.1$ ($p < 10^{-4}$; see Table 3 in Fan et al. 2016), which is used to estimate the X-ray luminosity for FSRQs without X-ray measurement.

In our sample, 393 sources have no measured redshift (157 BL Lacs and 236 BCUs). For these sources, we use the median values of the known redshifts of confirmed BL Lacs ($z = 0.359$) and confirmed FSRQs ($z = 1.108$) for unknown-redshift BL Lacs (including BCUs divided into BL Lacs) and BCUs divided into FSRQs, respectively. Finally, we have 803 BL Lacs and 589 FSRQs, of which the class type, redshift, and other parameters are presented in Table 1.

We note that there is only a blazar having extremely large synchrotron peak frequency above $> 10^{20}$ Hz in the sample: 3FGL J1504.5-8242 (1RXS J150537.1-824233) having $\log \nu_s^p(\text{Hz}) = 20.12$, which is a BCU (Acero et al. 2015; Fan et al. 2016). It has a γ -ray photon index $\Gamma_\gamma = 2.3$ (Acero et al. 2015), which is a typical value of FSRQs. According to the above criterion, this source is classified as a FSRQ. Its synchrotron peak frequency may be overestimated because of that the quality of its synchrotron broadband SED is bad³. For

³<http://ned.ipac.caltech.edu/>

this source, the synchrotron peak frequency is assumed to be an average value of FSRQs: $\log \nu_s^p(\text{Hz}) = 13.94$ (see Fan et al. 2016).

A one-zone synchrotron + IC model is adopted in this paper to estimate the jet physical parameters. This model assumes a homogeneous and isotropic emission region, which is a sphere with radius R , a uniform magnetic field with strength B , and a uniform electron energy distribution $N(\gamma)$. The emission region moves relativistically with a Lorentz factor $\Gamma = 1/\sqrt{1-\beta^2}$ and a viewing angle θ , which forms the Doppler factor $\delta = 1/[\Gamma(1-\beta\cos\theta)]$. The frequency and luminosity transform from jet to AGN frames as⁴, $\nu = \delta\nu'$ and $\nu L(\nu) = \delta^4\nu'L'(\nu')$, respectively. As stressed in Tavecchio et al. (1998), the jet parameters specifying the one-zone model are uniquely determined once the basic observables and variability time-scale are known. Therefore, along the lines of the analytical treatment in Tavecchio et al. (1998) for the one-zone SSC model, it is possible to derive a useful approximate analytical expression for the jet physical parameters as a function of the observed SED quantities (e.g., the peak frequency and luminosity of the synchrotron and IC components). Because of that the synchrotron emission at the peak frequency are usually optical thin, we have

$$L'_{sy}(\nu') = \frac{4}{3}\pi R^3 \cdot 4\pi j(\nu'), \quad (1)$$

where the emitting efficient is

$$j_{sy}(\nu') = \frac{1}{4\pi} \int N(\gamma) P_{sy}(\nu', \gamma) d\gamma. \quad (2)$$

Here $P_{sy}(\nu', \gamma)$ is the synchrotron emission power of a single electron. Because of that the SED of the synchrotron emission of a single electron is very narrow in the frequency space (see, e.g., Blumenthal & Gould 1970; Rybicki & Lightman 1979), one sometimes assumes that all emission is produced at a particular frequency, i.e., monochromatic approximation (see Chen 2017, for detail), using the following equation as an approximation of $P_{sy}(\nu', \gamma)$,

$$P_{sy}(\nu', \gamma) \approx \frac{4}{3}\sigma_{Tc}U_B\gamma^2\delta(\nu' - \frac{4}{3}\nu_L\gamma^2), \quad (3)$$

where $\nu_L = eB/2\pi m_e c$ is the Lamer frequency and $U_B = B^2/8\pi$ is the magnetic field energy density. In this case, the synchrotron luminosity (Equation 1) will be reduced to

$$L'_{sy}(\nu') = \frac{4}{3}\pi R^3 \cdot 4\pi \cdot \frac{\sigma_{Tc}U_B}{8\pi\nu_L}\gamma N(\gamma), \quad (4)$$

where $\nu' = (4/3)\nu_L\gamma^2$.

⁴The prime refers to values measured in the jet frame.

In leptonic blazar jet models, the synchrotron and IC emission components are radiations of nonthermal electron populations that are assumed to be isotropic in the jet fluid frame. One technique is to fit the data by injecting power-law electron distribution and allowing the electrons to evolve in response to radiative and adiabatic energy losses (e.g., Böttcher & Chiang 2002; Moderski et al. 2003; Katarzyński et al. 2003). In this case, many parameters must be specified, including the cutoff energies, injection indexes, and power, but this method is potentially useful to follow the dynamic spectral behavior of blazars. Contrary to this approach, we abandon any preconceptions about particle acceleration and employ the simplest functional form that is able to provide reasonably good fits to the SED data (see, e.g., Finke et al. 2008, for SSC modeling of TeV blazars with power-law electron distributions). For this purpose, and with the goal of minimizing the number of free parameters, a three-parameter log-parabolic function is employed to describe electron energy distribution in this paper (see Dermer et al. 2014; Fan et al. 2016),

$$N(\gamma) = N_0 \left(\frac{\gamma}{\gamma_0} \right)^{-3} 10^{-b \log^2 \left(\frac{\gamma}{\gamma_0} \right)}. \quad (5)$$

This electron energy distribution is only phenomenologically assumed to follow the log-parabola, without taking self-consistently into account the evolution due to injection and cooling effects (e.g., Kirk et al. 1998; Tramacere et al. 2011). Despite this, the log-parabolic model can successfully represent the broadband SED of blazars in both observation (single-source and sample studies; e.g., Massaro et al. 2004; Chen 2014; Dermer et al. 2015; Krauß et al. 2016; Xue et al. 2016; Fan et al. 2016) and theoretical SED modeling (e.g., Tramacere et al. 2011; Cerruti et al. 2013; Dermer et al. 2014; Yan et al. 2015; Ding et al. 2017; Hu et al. 2017). As for why there is a term $(\gamma/\gamma_0)^{-3}$, it is to guarantee that the electrons of γ_0 emit at the peak frequency in the $\log \nu' - \log \nu' L'_{\nu'}$ frame (see below). The entire description of the electron energy distribution is then given by three parameters: the normalization N_0 , the peak Lorentz factor γ_0 of nonthermal electrons, and the spectral curvature parameter b .

The curvature, b , of the electron energy distribution has a relation with that of the SED (synchrotron bump), $b \approx 5P_1$ (see, e.g., Massaro et al. 2006; Chen 2014). In this case, the synchrotron peak frequency in the $\log \nu' - \log \nu' L'_{\nu'}$ frame is

$$\nu'_{sy}{}^p \simeq (4/3) \nu_L \gamma_0^2, \quad (6)$$

and the corresponding peak luminosity is

$$\nu'_{sy}{}^p L'_{sy}(\nu'_{sy}{}^p) = 4\pi \frac{16}{9} \pi R^3 \frac{\sigma_{TC}}{8\pi} U_B N_0 \gamma_0^3. \quad (7)$$

For the jet opening angle θ_j , the causality condition requires $\theta_j \Gamma \lesssim 1$ (Clausen-Brown et al. 2013), which is also supported by numerical simulations of axisymmetric, magnetically

driven outflows (Komissarov et al. 2009), while constraints imposed by the SSC process (Nalewajko et al. 2014) and observations of radio cores (e.g., Jorstad et al. 2005; Pushkarev et al. 2009) indicate $\theta_j \Gamma \gtrsim 0.1 - 0.7$. In the calculations presented, we adopted a value of $\theta_j \Gamma = 1$, and in this case, we have $\delta \lesssim \Gamma$ (with a viewing angle of roughly $\theta \gtrsim \theta_j$), of which the exact values will not significantly affect our conclusions.

The SSC emission may account for the emission at the peak of the IC component of BL Lacs, while the EC emission may account for that of FSRQs. The emissions at the IC peak can be at the Thomson or Klein-Nishina (KN) regimes. We will discuss these cases separately. The variability timescale can set an upper limit on the size of the emission region due to the causality, $R \lesssim \delta c \Delta t / (1+z)$. The variability timescales are not required to be the same in various sources (see Ulrich et al. 1997, for a review; and e.g. Bonnoli et al. (2011) and Abdo et al. (2011) for the well-studied blazars 3C 454.3 and Mrk 421; and Nalewajko (2013) for a systematic study indicating a typical variability timescale in the source frame in the *Fermi*/LAT band of ≈ 1 day; see also Hu et al. (2014)), while for simplicity, the average value $\Delta t / (1+z) \approx 1$ day (in the source frame) is assumed in our calculation (e.g., Kang et al. 2014; Zhang et al. 2015).

3.1. SSC at the Thomson regime

In the case of Thomson scattering, the SSC peak frequency follows

$$\frac{\nu'_{ssc}}{\nu'_{sy}} = \frac{4}{3} \gamma_0^2. \quad (8)$$

Integrating the monochromatic luminosity (see Equations 4 and 5), one can get the total synchrotron luminosity,

$$L'_{sy} = \nu_{sy}^p L'_{sy}(\nu_{sy}^p) \sqrt{\frac{\pi \ln 10}{b/4}}. \quad (9)$$

Within the one-zone model, the average synchrotron energy density is (see Chen 2017),

$$U_{sy-Th} = \frac{9}{4} \frac{L'_{sy}}{4\pi R^2 c}. \quad (10)$$

Therefore, the SSC peak luminosity follows

$$\frac{\nu_{ssc}^p L'(\nu_{ssc}^p)}{\nu_{sy}^p L'(\nu_{sy}^p)} = \frac{U_{sy-Th}}{U_B} = \frac{\sigma_T}{2} \sqrt{\frac{\pi \ln 10}{b/4}} R N_0 \gamma_0^3. \quad (11)$$

Combining the Equations 6, 9, 8, 11, and

$$\begin{cases} \nu = \delta\nu' \\ \nu L(\nu) = \delta^4\nu' L'(\nu') \\ R = c\Delta t\delta/(1+z) \end{cases} \quad (12)$$

we have

$$\begin{cases} \gamma_0 = 8660.3 \left(\frac{\nu_{ssc}^p}{10^{23} \text{ Hz}} \frac{10^{15} \text{ Hz}}{\nu_{sy}^p} \right)^{1/2} \\ \delta = 9.0365 \left(\frac{\nu_{sy}^p L(\nu_{sy}^p)}{10^{45} \text{ erg/s}} \right)^{1/4} \left(\frac{\nu_{sy}^p}{10^{15} \text{ Hz}} \right)^{-1/2} \left(\frac{\nu_{ssc}^p L(\nu_{ssc}^p)}{\nu_{sy}^p L(\nu_{sy}^p)} \right)^{-1/4} \left(\frac{\nu_{ssc}^p}{10^{23} \text{ Hz}} \frac{10^{15} \text{ Hz}}{\nu_{sy}^p} \right)^{1/2} \left(\frac{\Delta t(1+z)}{1 \text{ day}} \right)^{-1/2} \left(\frac{b}{2} \right)^{-1/8} \\ B = 0.39533 \left(\frac{\nu_{sy}^p L(\nu_{sy}^p)}{10^{45} \text{ erg/s}} \right)^{-1/4} \left(\frac{\nu_{sy}^p}{10^{15} \text{ Hz}} \right)^{3/2} \left(\frac{\nu_{ssc}^p L(\nu_{ssc}^p)}{\nu_{sy}^p L(\nu_{sy}^p)} \right)^{1/4} \left(\frac{\nu_{ssc}^p}{10^{23} \text{ Hz}} \frac{10^{15} \text{ Hz}}{\nu_{sy}^p} \right)^{-3/2} \left(\frac{\Delta t(1+z)}{1 \text{ day}} \right)^{1/2} \left(\frac{b}{2} \right)^{1/8} \\ R = 2.3406 \times 10^{16} \left(\frac{\nu_{sy}^p L(\nu_{sy}^p)}{10^{45} \text{ erg/s}} \right)^{1/4} \left(\frac{\nu_{sy}^p}{10^{15} \text{ Hz}} \right)^{-1/2} \left(\frac{\nu_{ssc}^p L(\nu_{ssc}^p)}{\nu_{sy}^p L(\nu_{sy}^p)} \right)^{-1/4} \left(\frac{\nu_{ssc}^p}{10^{23} \text{ Hz}} \frac{10^{15} \text{ Hz}}{\nu_{sy}^p} \right)^{1/2} \left(\frac{\Delta t}{1 \text{ day}(1+z)^3} \right)^{1/2} \left(\frac{b}{2} \right)^{-1/8} \\ N_0 = 5.1991 \times 10^{-5} \left(\frac{\nu_{sy}^p L(\nu_{sy}^p)}{10^{45} \text{ erg/s}} \right)^{-1/4} \left(\frac{\nu_{sy}^p}{10^{15} \text{ Hz}} \right)^{1/2} \left(\frac{\nu_{ssc}^p L(\nu_{ssc}^p)}{\nu_{sy}^p L(\nu_{sy}^p)} \right)^{5/4} \left(\frac{\nu_{ssc}^p}{10^{23} \text{ Hz}} \frac{10^{15} \text{ Hz}}{\nu_{sy}^p} \right)^{-2} \left(\frac{\Delta t(1+z)}{1 \text{ day}} \right)^{-1/2} \left(\frac{b}{2} \right)^{5/8} \end{cases} \quad (13)$$

3.2. SSC at the KN regime

In the case of KN scattering ($\gamma_0 h\nu_{sy}^p \gtrsim m_e c^2$), the SSC peak frequency follows

$$\nu_{ssc}^p \approx \frac{2}{\sqrt{3}} \frac{\gamma_0 m_e c^2}{h}. \quad (14)$$

The effective SSC seed photon energy density can be easily derived through integrating from the minimum frequency to the critical frequency $\nu'_{sy-c} = (\sqrt{3}/2)(m_e c^2/h\gamma_0)$,

$$U_{sy-KN} = U_{sy-Th} \frac{1}{\sqrt{\pi}} \int_{t_c}^{+\infty} e^{-t^2} dt \quad (15)$$

where

$$t_c = \sqrt{\frac{b}{4 \ln 10}} \ln \left(\frac{h\nu_{sy}^p}{m_e c^2} \frac{h\nu_{ssc}^p}{m_e c^2} \right) \quad (16)$$

In the case of the KN regime, the SSC peak luminosity follows

$$\frac{\nu_{ssc}^p L'(\nu_{ssc}^p)}{\nu_{sy}^p L'(\nu_{sy}^p)} = \frac{U_{sy-KN}}{U_B} = \frac{\sigma_T}{2} \sqrt{\frac{\pi \ln 10}{b/4}} R N_0 \gamma_0^3 \frac{1}{\sqrt{\pi}} \int_{t_c}^{+\infty} e^{-t^2} dt. \quad (17)$$

Because of that the Equation 17 is actually an integral equation (t_c is a function of δ through $\nu_{sy,ssc}^p = \nu_{sy,ssc}^p/\delta$), the final estimated jet parameters cannot be analytically expressed as that in the Equation 13. The parameters (γ_0 , N_0 , B , δ , and R) can be derived through numerically solving the set of Equations 6, 9, 12, 14, and 17.

3.3. EC at the Thomson regime

The FSRQs usually have very strong emission from the BLR and dust torus, and these photons can be IC scattered by relativistic electrons in the jet. In the frame of the jet, the external photon energy density will be enhanced and the frequency will be amplified: $U'_{ext-Th} \approx (17/12)\Gamma^2 U_{ext}$ and $\nu'_{ext} \approx \Gamma\nu_{ext}$. In this case, the EC peak luminosity follows

$$\frac{\nu_{ec}^p L'(\nu_{ec}^p)}{\nu_{sy}^p L'(\nu_{sy}^p)} = \frac{U'_{ext-Th}}{U_B} \approx \frac{U_{ext}}{U_B} \frac{17}{12} \Gamma^2. \quad (18)$$

and the EC peak frequency,

$$\nu_{ec}^p \approx \frac{4}{3} \gamma_0^2 \Gamma \nu_{ext}. \quad (19)$$

Combining the Equations 6, 12, 18, and 19, we have (see also Chen & Bai 2011)

$$\frac{\nu_{ec}^p L(\nu_{ec}^p)}{\nu_{sy}^p L(\nu_{sy}^p)} = \frac{17e^2}{6\pi m_e^2 c^2} \frac{U_{ext}}{\nu_{ext}^2} \left(\frac{\nu_{ec}^p}{\nu_{sy}^p} \right)^2 \quad (20)$$

This means that the external photon properties (i.e., U_{ext}/ν_{ext}^2) will be determined when given the synchrotron/EC peak frequency and luminosity. For the BLR, the emission is mainly contributed by Ly α lines, $\nu_{ext-BLR} \approx 2 \times 10^{15}$ Hz (Ghisellini & Tavecchio 2009). The dust torus reprocesses the disk emission into the IR band. As indicated by *Spitzer* observations, the typical peak frequency of IR dust torus emission is around $\nu_{ext-IR} \approx 3 \times 10^{13}$ (Cleary et al. 2007; Ghisellini & Tavecchio 2009; Gu 2013). Following Ghisellini & Tavecchio (2009), the radiation from the reprocessed dust torus (IR) or BLR is described as a blackbody spectrum. The issue of whether the radiation regions are inside or outside the BLRs is highly debated. Considering the γ -ray photons can be absorbed via photon-photon pair production above $\gtrsim 10$ GeV of BLR emission (e.g., Liu & Bai 2006; Bai et al. 2009), some authors suggested that the emission region should be outside the BLR (e.g., Sikora et al. 2009; Tavecchio & Mazin 2009; Tavecchio et al. 2013). The broadband SED modeling of a large sample also suggests that the emission region may be outside the BLR for most sources (e.g., Kang et al. 2014). In this case, the IC/dust process will dominate the γ -ray emission (Ghisellini & Tavecchio 2009). In this paper, the IC/dust torus models are considered in our calculation.

We assume a the Doppler factor of $\delta = 1/\Gamma(1 - \beta \cos\theta) \approx \Gamma$ for the relativistic jet close to the line of sight in blazars with a viewing angle $\theta \lesssim 1/\Gamma$ (Jorstad et al. 2005; Pushkarev et al. 2009). Combining the Equations 6, 9, 11, 12, 18 (or the Equation 20), and 19, the jet parameters can be derived (the SSC emission in this case is within the Thomson

regime),

$$\left\{ \begin{array}{l} \gamma_0 = 1641.5 \left(\frac{\nu_{sy}^p}{10^{14} \text{ Hz}} \right)^{1/2} \left(\frac{\nu_{ec}^p}{10^{22} \text{ Hz}} \frac{10^{14} \text{ Hz}}{\nu_{sy}^p} \right)^{1/4} \left(\frac{\nu_{sy}^p L(\nu_{sy}^p)}{10^{46} \text{ erg/s}} \right)^{-1/8} \left(\frac{\nu_{ssc}^p L(\nu_{ssc}^p)}{\nu_{sy}^p L(\nu_{sy}^p)} \right)^{1/8} \left(\frac{\nu_{ext}}{3 \times 10^{13} \text{ Hz}} \right)^{-1/4} \left(\frac{\Delta t(1+z)}{1 \text{ day}} \right)^{1/4} \left(\frac{b}{2} \right)^{1/4} \\ \delta = 9.6321 \left(\frac{\nu_{ec}^p}{10^{22} \text{ Hz}} \frac{10^{14} \text{ Hz}}{\nu_{sy}^p} \right)^{1/4} \left(\frac{\nu_{sy}^p L(\nu_{sy}^p)}{10^{46} \text{ erg/s}} \right)^{1/8} \left(\frac{\nu_{ssc}^p L(\nu_{ssc}^p)}{\nu_{sy}^p L(\nu_{sy}^p)} \right)^{-1/8} \left(\frac{\nu_{ext}}{3 \times 10^{13} \text{ Hz}} \right)^{-1/4} \left(\frac{\Delta t(1+z)}{1 \text{ day}} \right)^{-1/4} \left(\frac{b}{2} \right)^{-1/16} \\ B = 1.0323 \left(\frac{\nu_{ec}^p}{10^{22} \text{ Hz}} \frac{10^{14} \text{ Hz}}{\nu_{sy}^p} \right)^{-3/4} \left(\frac{\nu_{sy}^p L(\nu_{sy}^p)}{10^{46} \text{ erg/s}} \right)^{1/8} \left(\frac{\nu_{ssc}^p L(\nu_{ssc}^p)}{\nu_{sy}^p L(\nu_{sy}^p)} \right)^{-1/8} \left(\frac{\nu_{ext}}{3 \times 10^{13} \text{ Hz}} \right)^{3/4} \left(\frac{\Delta t(1+z)}{1 \text{ day}} \right)^{-1/4} \left(\frac{b}{2} \right)^{-1/16} \\ R = 2.4949 \times 10^{16} \left(\frac{\nu_{ec}^p}{10^{22} \text{ Hz}} \frac{10^{14} \text{ Hz}}{\nu_{sy}^p} \right)^{1/4} \left(\frac{\nu_{sy}^p L(\nu_{sy}^p)}{10^{46} \text{ erg/s}} \right)^{1/8} \left(\frac{\nu_{ssc}^p L(\nu_{ssc}^p)}{\nu_{sy}^p L(\nu_{sy}^p)} \right)^{-1/8} \left(\frac{\nu_{ext}}{3 \times 10^{13} \text{ Hz}} \right)^{-1/4} \left(\frac{\Delta t(1+z)}{1 \text{ day}} \right)^{3/4} \left(\frac{b}{2} \right)^{-1/16} \\ N_0 = 7.1622 \times 10^{-3} \left(\frac{\nu_{sy}^p}{10^{14} \text{ Hz}} \right)^{-3/2} \left(\frac{\nu_{ec}^p}{10^{22} \text{ Hz}} \frac{10^{14} \text{ Hz}}{\nu_{sy}^p} \right)^{-1} \left(\frac{\nu_{sy}^p L(\nu_{sy}^p)}{10^{46} \text{ erg/s}} \right)^{1/4} \left(\frac{\nu_{ssc}^p L(\nu_{ssc}^p)}{\nu_{sy}^p L(\nu_{sy}^p)} \right)^{3/4} \left(\frac{\nu_{ext}}{3 \times 10^{13} \text{ Hz}} \right) \left(\frac{\Delta t(1+z)}{1 \text{ day}} \right)^{-3/2} \\ U_{ext} = 3.2260 \times 10^{-4} \left(\frac{\nu_{ec}^p L(\nu_{ec}^p)}{\nu_{sy}^p L(\nu_{sy}^p)} \right) \left(\frac{\nu_{ec}^p}{10^{22} \text{ Hz}} \frac{10^{14} \text{ Hz}}{\nu_{sy}^p} \right)^{-2} \left(\frac{\nu_{ext}}{3 \times 10^{13} \text{ Hz}} \right)^2 \end{array} \right. \quad (21)$$

3.4. EC at the KN regime

In the case of the KN regime ($\gamma_0 \Gamma h \nu_{ext} \gtrsim m_e c^2$), the EC peak frequency is

$$\nu_{ec}^p \approx \frac{2}{\sqrt{3}} \frac{\gamma_0 m_e c^2}{h}. \quad (22)$$

The effective EC seed photon energy density can be easily calculated through integrating from the minimum frequency to the critical frequency $\nu'_{ext-c} = (\sqrt{3}/2)(m_e c^2/h\gamma_0)$,

$$U'_{ext-KN} = U'_{ext-Th} \frac{15}{\pi^4} \int_0^{x_c} \frac{x^3}{e^x - 1} dx, \quad (23)$$

where⁵,

$$x_c = 2.82 \frac{m_e^2 c^2}{h \nu_{ext}} \frac{m_e^2 c^2}{h \nu_{ec}}. \quad (24)$$

In the case of the KN regime, the EC peak luminosity follows

$$\frac{\nu_{ec}^p L'(\nu_{ec}^p)}{\nu_{sy}^p L'(\nu_{sy}^p)} = \frac{U'_{ext-KN}}{U_B} = \frac{U_{ext}}{U_B} \frac{17}{12} \Gamma^2 \int_0^{x_c} \frac{x^3}{e^x - 1} dx. \quad (25)$$

Combining the Equations 6, 9, 11, 12, and 22, we have (the SSC in this case is within

⁵The factor 2.82 accounts for the difference between the peak frequency of the blackbody spectrum and the kT/h .

the Thomson regime)

$$\left\{ \begin{array}{l} \gamma_0 = 61460 \left(\frac{\nu_{sy}^p L(\nu_{sy}^p)}{10^{46} \text{erg/s}} \right)^{-1/8} \left(\frac{\nu_{ssc}^p L(\nu_{ssc}^p)}{\nu_{sy}^p L(\nu_{sy}^p)} \right)^{1/8} \left(\frac{\nu_{sy}^p}{10^{17} \text{Hz}} \right)^{1/4} \left(\frac{\nu_{ec}^p}{10^{26} \text{Hz}} \frac{10^{17} \text{Hz}}{\nu_{sy}^p} \right)^{1/2} \left(\frac{\Delta t(1+z)}{1 \text{day}} \right)^{1/4} \left(\frac{b}{2} \right)^{1/16} \\ \delta = 11.404 \left(\frac{\nu_{sy}^p L(\nu_{sy}^p)}{10^{46} \text{erg/s}} \right)^{1/8} \left(\frac{\nu_{ssc}^p L(\nu_{ssc}^p)}{\nu_{sy}^p L(\nu_{sy}^p)} \right)^{-1/8} \left(\frac{\nu_{sy}^p}{10^{17} \text{Hz}} \right)^{-1/4} \left(\frac{\nu_{ec}^p}{10^{26} \text{Hz}} \frac{10^{17} \text{Hz}}{\nu_{sy}^p} \right)^{1/2} \left(\frac{\Delta t(1+z)}{1 \text{day}} \right)^{-1/4} \left(\frac{b}{2} \right)^{-1/16} \\ B = 0.62198 \left(\frac{\nu_{sy}^p L(\nu_{sy}^p)}{10^{46} \text{erg/s}} \right)^{1/8} \left(\frac{\nu_{ssc}^p L(\nu_{ssc}^p)}{\nu_{sy}^p L(\nu_{sy}^p)} \right)^{-1/8} \left(\frac{\nu_{sy}^p}{10^{17} \text{Hz}} \right)^{3/4} \left(\frac{\nu_{ec}^p}{10^{26} \text{Hz}} \frac{10^{17} \text{Hz}}{\nu_{sy}^p} \right)^{-3/2} \left(\frac{\Delta t(1+z)}{1 \text{day}} \right)^{-1/4} \left(\frac{b}{2} \right)^{-1/16} \\ R = 2.9539 \times 10^{16} \left(\frac{\nu_{sy}^p L(\nu_{sy}^p)}{10^{46} \text{erg/s}} \right)^{1/8} \left(\frac{\nu_{ssc}^p L(\nu_{ssc}^p)}{\nu_{sy}^p L(\nu_{sy}^p)} \right)^{-1/8} \left(\frac{\nu_{sy}^p}{10^{17} \text{Hz}} \right)^{-1/4} \left(\frac{\nu_{ec}^p}{10^{26} \text{Hz}} \frac{10^{17} \text{Hz}}{\nu_{sy}^p} \right)^{1/2} \left(\frac{\Delta t(1+z)}{1 \text{day}} \right)^{3/4} \left(\frac{b}{2} \right)^{-1/16} \\ N_0 = 1.1526 \times 10^{-7} \left(\frac{\nu_{sy}^p L(\nu_{sy}^p)}{10^{46} \text{erg/s}} \right)^{1/4} \left(\frac{\nu_{ssc}^p L(\nu_{ssc}^p)}{\nu_{sy}^p L(\nu_{sy}^p)} \right)^{3/4} \left(\frac{\nu_{sy}^p}{10^{17} \text{Hz}} \right)^{-1/2} \left(\frac{\nu_{ec}^p}{10^{26} \text{Hz}} \frac{10^{17} \text{Hz}}{\nu_{sy}^p} \right)^{-2} \left(\frac{\Delta t(1+z)}{1 \text{day}} \right)^{-3/2} \left(\frac{b}{2} \right)^{3/8} \end{array} \right. \quad (26)$$

After getting these parameters, the external energy density, U_{ext} , can be easily derived through combining the Equations 12 and 25.

As discussed above, we use the SSC model for all BL Lacs and the EC model for all FSRQs. The input parameters include ν_{sy}^p , $\nu_{ssc/ec}^p$, $\nu_{sy}^p L(\nu_{sy}^p)$, $\nu_{ssc}^p L(\nu_{ssc}^p)$ and P_1 . The criterion from the Thomson to KN regimes in the SSC model is $\gamma_0 h \nu_{sy}^p \gtrsim m_e c^2$ (see Section 3.2), and that in the EC model is $\gamma_0 \Gamma h \nu_{ext} \gtrsim m_e c^2$ (see Section 3.4).

4. Results and Discussion

the *COS B* satellite first detected 3C 273 as a γ -ray blazar (Swanenburg et al. 1978). After that, nearly 100 blazars were discovered by the Energetic Gamma-Ray Experiment Telescope (EGRET) onboard the *Compton Gamma Ray Observatory* (Hartman et al. 1999; Nandikotkur et al. 2007). The 20-fold (sensitivity) improvement of *Fermi*/LAT has now detected more than 1000 blazars, which allows us to do population studies. For all 1392 γ -ray blazars in our sample, we estimate the jet physical parameters.

We firstly calculate the Doppler factor (δ) and the size of the emission region (R), for which (histogram) distributions are presented in Figure 3. It can be seen that R and δ follow the same distributions, which is due to the assumptions $R \lesssim \delta c \Delta t / (1+z)$ and $\Delta t / (1+z) \approx 1$ day in our calculation. The median values of the Doppler factors of FSRQs, BL Lacs, and total blazars are $\delta \simeq 10.7$, 22.3, and 13.1, respectively. The significantly larger of δ of BL Lacs relative to that of FSRQs seems to be inconsistent with estimations from other methods. The independent methods found that the Doppler factors of BL Lacs are comparable with or even smaller than those of FSRQs, such as from radio variability (Lähtenmäki & Valtaoja 1999; Fan et al. 2009; Savolainen et al. 2010; Liodakis et al. 2017), SED modeling (Ghisellini et al. 1998, 1993), pair production (Mattox et al. 1993; Fan et al. 2014), or apparent superluminal motions (Jorstad et al. 2005; Hovatta et al. 2009). From

Figure 3, we find that some BL Lacs present extremely large values of δ , even reaching $\sim 10^4$, which values may be incorrect for blazars. The typical values of the Doppler factor in blazars range from a few to ~ 50 based on various methods as mentioned above (e.g., Lähteenmäki & Valtaoja 1999; Fan et al. 2009; Savolainen et al. 2010; Liodakis et al. 2017; Ghisellini et al. 1998, 1993; Mattox et al. 1993; Fan et al. 2014; Jorstad et al. 2005; Hovatta et al. 2009; Ghisellini et al. 2014; Ghisellini & Tavecchio 2015). There is also a small fraction of BL Lacs having very low values of Doppler factor ($\delta < 1$). In our model, the Doppler factor is assumed to be equal to the jet bulk Lorentz factor $\delta = \Gamma$, which must be larger than 1. For these sources with extreme Doppler factors, the estimations of other jet parameters may also be incorrect. We calculate the median value of the Doppler factors of all BL Lacs with $1 < \delta < 100$, which gives $\delta_m \simeq 14.3$. This median value is used for 268 BL Lacs with extreme Doppler factors ($\delta < 1$ or $\delta > 100$) and determining other jet parameters. In this case, δ is a new input parameter other than ν_{sy}^p , ν_{ssc}^p , $\nu_{sy}^p L(\nu_{sy}^p)$, $\nu_{ssc}^p L(\nu_{ssc}^p)$, and P_1 . Due to the large uncertainty of the estimation of ν_{ssc}^p (see Abdo et al. 2010, and discussion below), we therefore use δ instead of ν_{ssc}^p as the input parameter to calculate other jet parameters. There are no FSRQs having $\delta > 100$ and only three FSRQs having $\delta < 1$. We use the same method to determine the other jet parameters of these three FSRQs (using $\delta_m \simeq 10.7$, the median value of δ of all FSRQs with $\delta > 1$). We calculate all jet parameters and present them in Table 1, where sources with $\delta < 1$ or $\delta > 100$ are labeled with an asterisk. The full version of the Table 1 is available in online ASCII form, which can be downloaded publicly. In the Figure 4, we present the (histogram) distributions of some jet parameters, and the median values of these are listed in Table 2.

The upper left panel in Figure 4 is the distribution of the electron peak energy γ_0 . The red line refers to FSRQs, the blue line indicates BL Lacs, and the black dashed line is for the total blazars. It clearly shows two separated populations/dichotomic distributions for FSRQs and BL Lacs, with median values $\gamma_0 \simeq 1167.8$ and 12077, respectively, which are comparable to previous studies⁶ (e.g., Zhang et al. 2015; Ghisellini & Tavecchio 2015; Qin et al. 2017). The median value for total blazars is $\gamma_0 \simeq 3646.1$. These separated populations between FSRQs and BL Lacs are actually results from the separated distribution of synchrotron peak frequency (also for the IC component) between FSRQs and BL Lacs, which are presented in Figure 5. These separated populations may reflect that FSRQs and BL Lacs are different in nature. As discussed above, the high accretion rate makes FSRQs usually luminous AGNs having very strong line / dust torus emission. Therefore, nonthermal electrons in the jets of FSRQs will suffer efficient cooling and attain a smaller typical energy. The

⁶The median value of $\gamma_0 \simeq 1167.8$ of FSRQs in this paper is slightly larger than the previous result, where γ_0 ranges from 100 to 1000 (e.g., Zhang et al. 2015; Ghisellini & Tavecchio 2015).

low accretion rate makes BL Lacs low-luminosity AGNs, with no or very weak emission lines. Therefore, the electrons in BL Lac jets suffer less cooling, which leads to a larger typical energy. These results are consistent with the so-called blazar sequence (see, e.g., Fossati et al. 1998; Ghisellini et al. 1998; Chen & Bai 2011). Blazars were classified as low-, intermediate-, and high-synchrotron-peaked (LSP, ISP, and HSP) blazars based on their synchrotron peak frequency by Abdo et al. (2010) and later by Fan et al. (2016) based on their Bayesian classification of peak frequency for a larger sample of *Fermi*/LAT-detected blazars. From LSP to HSP blazars, the luminosity forms a gradual decreasing trend, which is called the blazar sequence (Fossati et al. 1998; Ghisellini et al. 1998; Chen & Bai 2011). However, some authors claimed that this sequence was from a selection effect, because after being corrected by the Doppler-beaming effect, the negative correlation between the peak frequency and luminosity disappeared (see Nieppola et al. 2008; Wu et al. 2009; Fan et al. 2017). The IC emission of smaller-energy electrons in FSRQs corresponds to softer γ -ray emission, while the higher-energy electrons in BL Lacs produce harder γ -ray emission. This is consistent with the fact that FSRQs and BL Lacs are distributed at two separate areas in the $L_\gamma - \Gamma$ plane, as shown in Figure 2 (see also Ghisellini et al. 2009; Abdo et al. 2009; Ackermann et al. 2015).

The distribution of the magnetic field is shown in the upper right panel of Figure 4. The median values of FSRQs, BL Lacs, and total blazars are $B \simeq 1.56, 0.119,$ and 0.446 Gs, respectively. These values are roughly consistent with the blazar sample SED modeling results (Ghisellini & Tavecchio 2015), in which the typical value of the magnetic field strength of FSRQs are found to range from 1 to 10 Gs and BL Lacs widely range from 0.001 to 10 Gs (see, e.g., Tavecchio et al. 2010; Zhang et al. 2012; Costamante et al. 2017).

The distribution of the curvature b of the electron energy distribution (see Equation 5) is presented in the bottom left panel of Figure 4. Note that we calculate this parameter $b = 5P_1$, where P_1 is the curvature of the observed SED of the synchrotron component, whose values are given by Fan et al. (2016). The median value of FSRQs ($b \simeq 0.6$) is only slightly larger than that of BL Lacs ($b \simeq 0.55$), with the median of total blazars $b \simeq 0.55$ (see Chen 2014).

The uncertainty of the estimation of these parameters comes from the input parameters. An important contribution comes from the IC peak frequency ν_{IC}^p , which is derived from the γ -ray photon index through $\log \nu_{IC}^p = -4\Gamma + 31.6$ (Equation 5 in Abdo et al. 2010). As proposed by Abdo et al. (2010), the error of the estimated $\log \nu_{IC}^p$ is about ~ 0.7 , which leads to uncertainty of the estimated jet parameters. For the SSC model, we have a corresponding uncertainty about $\Delta \log \gamma_0 \sim 0.35, \Delta \log \delta \sim 0.35, \Delta \log B \sim 1.05$ and $\Delta \log R \sim 0.35$ (simply for Thomson scattering; see Equation 13). For the EC model, we have a corresponding

uncertainty about $\Delta \log \gamma_0 \sim 0.175$, $\Delta \log \delta \sim 0.175$, $\Delta \log B \sim 0.525$ and $\Delta \log R \sim 0.175$ (simply for Thomson scattering; see Equation 21).

4.1. Disk-jet Connection and Jet Launching

The most promising scenario for launching astrophysical relativistic jets involves large-scale magnetic fields anchored in rapidly rotating compact objects. The idea of driving outflows by rotating magnetic fields, originally invented by Weber & Davis (1967) to explain the spindown of young stars, was successfully applied to pulsar winds (Michel 1969) and became a dominant mechanism in theories of relativistic jets in AGNs (Lovelace et al. 1987; Li et al. 1992; Vlahakis & Königl 2004) and γ -ray bursts (e.g., Spruit et al. 2001; Vlahakis & Königl 2001). Powerful jets in AGNs can be powered by the innermost portions of accretion disks and/or by rapidly rotating BHs (Blandford & Znajek 1977; Blandford & Payne 1982; Spruit 2010). The correlation between the jet and the accretion disk/BLR has been presented in many studies (e.g., Cao & Jiang 1999; Ho & Peng 2001; Wang et al. 2003; Ghisellini et al. 2014; Liu et al. 2014; Sbarrato et al. 2016; Du et al. 2016). Because the disk continuum and line emission are usually missing in BL Lacs, we study the jet-disk connection only for FSRQs through comparing the accretion (e.g., accretion disk/BLR/BH mass) with the jet properties.

The disk bolometric luminosity L_{bol} can be derived from a continuum luminosity based on the empirical relation (Shen et al. 2011). In order to avoid contamination by the non-thermal continuum, the accretion disk luminosity can be derived from the luminosity of broad emission lines as a proxy of $L_{\text{disk}} \approx 10L_{\text{BLR}}$ (Calderone et al. 2013), and the total luminosity of broad emission lines can be reconstructed through visible broad lines (see, e.g., Francis et al. 1991; Vanden Berk et al. 2001). $H\beta$, Mg II, and C IV (Shaw et al. 2012) are widely used to scale to the quasar template spectrum of Francis et al. (1991) to calculate the total BLR luminosity L_{BLR} . In Francis et al. (1991), the Ly α is used as a reference of 100, and the total relative BLR flux is 555.77, of which $H\beta$ is 22, Mg II is 34 and C IV is 63 (see also, e.g., Vanden Berk et al. 2001; Ghisellini et al. 2014). The BH mass and accretion rate are fundamental parameters of AGNs. The virial method is now the most widely used to estimate the BH mass (e.g., Gu et al. 2001; Wu et al. 2004; Greene & Ho 2005). The uncertainty of a BH mass derived in this way is a factor of $\sim 3 - 4$ (Vestergaard & Peterson 2006). Other methods include using the relation between BH mass and stellar velocity dispersion (e.g., Wu et al. 2002) and between BH mass and host-galaxy bulge luminosity (e.g., Laor 2001). Shaw et al. (2012) reported the optical spectroscopy of a large sample of γ -ray-detected blazars, and estimated their BH mass through the virial method. We collect their

available data (BH mass and emission lines) for our sample and finally get 144 FSRQs. As in the method discussed above, we use their optical emission lines to scale to the quasar template spectrum to calculate the total BLR luminosity. Because of that the BLR luminosities derived from various emission lines are consistent with each other (e.g., Francis et al. 1991; Shen et al. 2011; Shaw et al. 2012), we use the average value of the BLR luminosity if more than one emission line is available. The disk luminosity is then derived by $L_{\text{disk}} \approx 10L_{\text{BLR}}$. Shen et al. (2011) studied the properties of quasars in the Sloan Digital Sky Survey Data Release 7 catalog. They calculated the virial BH mass and bolometric luminosity L_{bol} through the correlation between L_{bol} and continuum luminosity as presented in Richards et al. (2006). The disk luminosity can be calculated $L_{\text{disk}} = L_{\text{bol}}/2$ (see Calderone et al. 2013). We further compile available data from Shen et al. (2011), and get another 46 FSRQs with disk luminosity and 44 FSRQs with BH mass. We note that some famous FSRQs are not included in these samples, e.g., 3C 273 and 3C 454.3. We then search the literature for FSRQs with well-measured disk luminosity and BH mass (Xiong & Zhang 2014). Finally, we have 232 FSRQs with measured disk luminosity and 229 with measured BH mass, 222 FSRQs have both values. The 3 FSRQs with Doppler factors $\delta < 1$ are not included in these sources.

Integrating the observed broadband SED, including both synchrotron and IC components, we can calculate the jet bolometric luminosity L_{obs} . The Figure 6 shows L_{obs} as a function of L_{disk} for the 232 FSRQs with well-measured disk luminosity. These show a robust correlation⁷ $\log L_{\text{disk},46} = (0.788 \pm 0.076) \log L_{\text{obs},46} - (1.44 \pm 0.14)$ (solid blue line) with a chance probability $p = 4.76 \times 10^{-15}$ (Pearson test). The black dotted line represents $L_{\text{obs}} = L_{\text{disk}}$ and the black dashed line $L_{\text{obs}} = 100L_{\text{disk}}$, which indicates that the jet bolometric luminosity is of the order of ~ 100 times the disk luminosity $L_{\text{obs}} \approx 100L_{\text{disk}}$. The entire radiation power of the jet can be estimated through $P_{\text{r}} = 2L_{\text{obs}}\Gamma^2/\delta^4 \approx 2L_{\text{obs}}/\delta^2$, which is the power that the jet expends in producing the nonthermal radiation. Based on VLBI-detected superluminal motion, or broadband SED model, the jet Doppler factor is found to be an order of $\delta \gtrsim 10$ (e.g., Lister et al. 2013; Ghisellini & Tavecchio 2015). Our estimation gives a median value of $\delta = 10.7$ for FSRQs (see the discussion above and/or the upper left panel of Figure 4). In this case, we have the entire jet radiation power will be on the order of the disk luminosity $P_{\text{r}} \approx L_{\text{disk}}$. The jet radiative efficiency is believed to be on the order of $P_{\text{r}}/P_{\text{jet}} \sim 10\%$, which holds for AGNs, γ -ray bursts, and even for BH X-ray binaries (Nemmen et al. 2012; Zhang et al. 2013; Ma et al. 2014), which gives an inevitable consequence that the jet power, $P_{\text{jet}} \approx 10P_{\text{r}}$, is larger than the disk luminosity, $P_{\text{jet}} \approx 10L_{\text{disk}}$. This suggests that the jet-launching processes and the way of transporting energy from the vicinity of the BH to infinity must be very efficient.

⁷ $L_{\text{disk},46} = (L_{\text{disk}}/10^{46}) \text{ erg s}^{-1}$ and $L_{\text{obs},46} = (L_{\text{obs}}/10^{46}) \text{ erg s}^{-1}$.

The relativistic jet may be driven from the rapidly rotating BH. Increasing the spin of the BH shrinks the innermost stable orbit while increasing the accretion disk radiative efficiency $\eta_{\text{acc}} = L_{\text{disk}}/\dot{M}c^2$ to a maximum value $\eta_{\text{acc}} \approx 0.3$ (Thorne 1974), where \dot{M} is the mass accretion rate. Assuming the accretion disk radiative efficiency $\eta_{\text{acc}} = 0.3$, we calculate the accretion power $L_{\text{acc}} = \dot{M}c^2 = L_{\text{disk}}/\eta_{\text{acc}}$ (same as that in, e.g., Ghisellini et al. 2014).

With the jet physical parameters, we calculate the jet power through⁸, $P_{\text{jet}} = 2\pi R^2 c\Gamma^2(U_{\text{B}} + U_{\text{e}} + U_{\text{p}})$, where U_{e} and U_{p} are the electron and proton energy density in the jet comoving frame (see, e.g., Celotti & Ghisellini 2008; Ghisellini et al. 2014). We adopt the conventional assumption that jet power is carried by electrons and protons (with one cold proton per emitting electron). In this case, U_{e} and U_{p} can be easily derived for the log-parabolic distribution of electrons (see Equation 5): $U_{\text{e}} = \int N(\gamma)\gamma m_{\text{e}}c^2 d\gamma = N_0\gamma_0^2 m_{\text{e}}c^2 \sqrt{\pi \log 10/b} 10^{1/4b}$ and $U_{\text{p}} = m_{\text{p}}c^2 \int N(\gamma) d\gamma = N_0\gamma_0 m_{\text{p}}c^2 \sqrt{\pi \log 10/b} 10^{1/b}$. The existence of electron-positron pairs would reduce the jet power. Note that the median value of $\gamma_0 = 1167.8$ is near the mass ratio of proton to electron, $m_{\text{p}}/m_{\text{e}}$, implying that the jet power will not reduce significantly when considering electron-positron pairs. In addition, pairs cannot largely outnumber protons, because otherwise the Compton rocket effect would stop the jet (see, e.g., Ghisellini & Tavecchio 2010).

In order to study the relations among the jet and accretion disk, we plot the accretion power as a function of the jet power in the Figure 7 (upper panel). The solid blue line shows the best-fit relation⁹: $\log L_{\text{acc},46} = (2.25 \pm 0.27) \log P_{\text{jet},46} - (0.34 \pm 0.12)$ (the Pearson test shows a chance probability $p = 2.85 \times 10^{-11}$). The dashed black line is the equality line. This result shows that a significant number of FSRQs have jet power greater than the accretion power, supported by the distribution of the ratio of jet power to accretion power ($P_{\text{jet}}/L_{\text{acc}}$) as shown in the left panel of Figure 8, implying that accretion power is not sufficient to launch the jets. The production of such large-power jet cannot be treated as a marginal by-product of the accretion disk flow and most likely is governed by the BZ mechanism (Blandford & Znajek 1977). The gravitational energy released from accretion cannot only be transformed into heat and radiation but also powers jets through the BP process (Blandford & Payne 1982). In addition, the gravitational energy can also amplify the magnetic field, allowing the field to access the rotational energy of the BH and transform part of it into powerful jets through the BZ process (Blandford & Znajek 1977). As revealed by recently general relativistic magnetohydrodynamical (MHD) numerical simulations (e.g., Tchekhovskoy et al. 2011; McKinney et al. 2012; Li 2014), the average outflowing jet/wind

⁸The factor of 2 accounts for the two jets.

⁹ $L_{\text{acc},46} = (L_{\text{acc}}/10^{46}) \text{ erg s}^{-1}$ and $P_{\text{jet},46} = (P_{\text{jet}}/10^{46}) \text{ erg s}^{-1}$.

power can even exceed the total accretion power for the case of spin value $a = 0.99$ when the BZ process dominates. The magnetic flux required to explain the production of the most powerful jets has been found to agree with the maximum magnetic flux that can be confined on BHs by the ram pressure of “magnetically arrested disks” (MAD) (Narayan et al. 2003). In recent years, the MAD scenario has been thoroughly investigated and is now considered to be the likely remedy for the production of very powerful jets (Tchekhovskoy et al. 2011; McKinney et al. 2012; Sikora & Begelman 2013). However, as numerical simulations suggest, the powers of the jets launched in the MAD scenario depend not only on the spin and magnetic flux but also on the disk’s geometrical thickness (Avara et al. 2016), with the jet power scaling approximately quadratically with all of these quantities (Sikora 2016). This large power of the relativistic jet in some FSRQs suggests that the BZ process will dominate the jet launching, which confirms some previous studies (see, e.g., Zamaninasab et al. 2014; Ghisellini et al. 2014).

The middle panel of Figure 7 indicates jet power as a function of Eddington luminosity, $L_{\text{Edd}} = 1.26 \times 10^{38} (M/M_{\odot}) \text{ erg s}^{-1}$, for 229 sources with measured BH mass, which presents a significant correlation with the best linear fitting¹⁰ $\log L_{\text{Edd},46} = (1.38 \pm 0.14) \log P_{\text{jet},46} + (0.220 \pm 0.064)$ (solid blue line) and a chance probability $p = 4.0 \times 10^{-14}$ (the Pearson test). The black dashed line is for the equality line, which shows that the jet power in units of Eddington luminosity is less than 1 for most sources. This is supported by the distribution of the ratio of jet power to Eddington luminosity, as shown in the right panel of Figure 8, with a median value of 0.382.

The bottom panel of Figure 7 shows a relation between the Eddington ratio (defined as $\lambda = L_{\text{disk}}/L_{\text{Edd}}$) and jet power, suggesting almost no correlation between these two parameters (the Pearson test gives $r = 0.144$ and $p = 0.0325$; see, e.g., Zhang et al. 2015, for similar results of FSRQs). This suggests that the accretion rate may not be very important for driving the jet. As discussed above, this is consistent with the idea that these jets may not be launched through the BP process, related to the accretion process, but rather through the BZ process extracting the rotational energy of the BH. Actually, BL Lacs are believed to have very weak disk continuum emission and low accretion rates compared with FSRQs (Cao 2002; Xu et al. 2009; Ghisellini et al. 2009; Falomo et al. 2014). BL Lacs have comparable (very slightly lower) jet powers with FSRQs (the median values $P_{\text{jet}} = 20.0, 6.30,$ and $12.0 \times 10^{45} \text{ erg s}^{-1}$ for FSRQs, BL Lacs, and total blazars, respectively; see discussion next subsection, the Table 2 and/or the bottom right panel of Figure 4). Therefore, one may expect that the noncorrelation between Eddington ratio and jet power will extend down to

¹⁰ $L_{\text{Edd},46} = (L_{\text{Edd}}/10^{46}) \text{ erg s}^{-1}$.

the low Eddington ratio tail when considering BL Lacs.

The distribution of Eddington ratio ($L_{\text{disk}}/L_{\text{Edd}}$) is presented in the left panel of Figure 8, with a median value of 0.148, consistent with previous results (e.g., Ghisellini et al. 2014). This implies that FSRQs have the standard geometrically thin, optically thick accretion disk (Shakura & Sunyaev 1973), which can launch powerful jets, contrary to some expectations (e.g., Livio et al. 1999; Meier 2002).

4.2. Jet Magnetization and Energy Transportation

The most diverse opinions about the nature of AGN relativistic jets concern their magnetic field and magnetization $\sigma = P_{\text{B}}/P_{\text{kin}}$, where P_{B} and P_{kin} are the magnetic and kinetic power, respectively. As discussed above, the current picture describing the powerful jet launching is that the jet can be produced from the central accretion system through the BZ mechanism by extracting BH rotation energy. This process is attributed to a key role of the dynamically important magnetic field, by means of which the BH spin energy is extracted and channeled into a Poynting/magnetic flux (Blandford & Znajek 1977; Tchekhovskoy et al. 2009, 2011). This magnetic flux cannot be developed by dynamo mechanisms in standard radiation-dominated accretion disks (Ghosh & Abramowicz 1997). However, such a flux is expected to be accumulated in the inner regions of the accretion flow and/or on the BH by the advection of magnetic fields from external regions (see Sikora & Begelman 2013; Cao & Spruit 2013, and references therein). In fact, the magnetic flux close to the BH horizon is so large that accretion likely occurs through a MAD flow, as discussed above (Narayan et al. 2003; Tchekhovskoy et al. 2011; McKinney et al. 2012). Starting as Poynting flux-dominated outflows, the jets are smoothly accelerated as magnetic power is being progressively converted to kinetic power and their magnetization drops, until a substantial equipartition between the magnetic and the kinetic power is established ($\sigma \approx 1$; see, e.g., Komissarov et al. 2007; Tchekhovskoy et al. 2009; Vlahakis 2015, and references therein). Therefore, at the end of this acceleration phase, the jet should still carry a substantial fraction (\approx half) of its power in the form of a Poynting flux. The jet acceleration becomes inefficient when $\sigma \lesssim 1$, from which point on, in the ideal MHD picture, σ will decrease logarithmically (Lyubarsky 2010).

However, even though blazars can have jets originating from MADs and be powered by the BZ mechanism, at the same time, they can have $\sigma \ll 1$ at the radio core and/or the blazar zone (i.e., the region where most of the radiation is produced, as indicated by blazar models with jet opening angles $1/\Gamma$; Nalewajko et al. 2014; Janiak et al. 2015; Zdziarski et al. 2015). Zdziarski et al. (2015) suggested that the magnetic-to-kinetic energy flux conver-

sion is assumed to result from the differential collimation of poloidal magnetic surfaces, which is the only currently known conversion mechanism in steady-state, axisymmetric, and nondissipative jets¹¹ (the conversion process can initially proceed quite efficiently; see also Tchekhovskoy et al. 2009; Lyubarsky 2010). Hence, it is likely that other mechanisms are involved in the conversion process working at $\sigma \lesssim 1$, such as MHD instabilities (see Komissarov 2011, and references therein), randomization of magnetic fields (Heinz & Begelman 2000), reconnection of magnetic fields (Drenkhahn & Spruit 2002; Lyubarsky 2010) and/or impulsive modulation of jet production (Lyutikov & Lister 2010; Granot et al. 2011). Little is known about the feasibility and efficiency of these processes in the context of AGNs. The MHD instabilities can develop when σ drops to unity or even earlier if stimulated by high-amplitude fluctuations of the jet power and direction, which are predicted in the MAD model (e.g., McKinney et al. 2012). In this case, the magnetization can reach $\sigma \ll 1$ even prior to the radio core and/or the blazar zone.

Studies of the σ parameter are important, not only for better understanding of the dynamical structure and evolution of relativistic jets but also because its value determines the dominant particle acceleration mechanism and its efficiency. Dissipation of part of the kinetic (through shocks) and/or magnetic (through reconnection) power leads to the acceleration of particles up to ultrarelativistic energies, producing the nonthermal emission we observe from blazars. Both versions (the first/second order) of Fermi acceleration were, and still are, commonly invoked as responsible for the ultrarelativistic electrons in AGN jets (see, e.g., Hoshino et al. 1992; Sironi & Spitkovsky 2011; Marscher 2014). Based on so-called particle-in-cell simulations, it is shown that electrons can be efficiently heated in very low magnetized jets ($\sigma \ll 1$; Madejski & Sikora 2016). The reconnection of magnetic energy is also a promising mechanism for particle acceleration in AGN jets (e.g., Giannios et al. 2009; Uzdensky 2011; Cerutti et al. 2012). A prediction of this scenario, resulting from detailed particle-in-cell simulations, is the substantial equipartition between the magnetic field and the accelerated electrons downstream of the reconnection site, where particles cool and emit the radiation we observe. For example, relativistic reconnection 2D models predict a lower limit of the order of $\sigma \sim 0.3$ in the dissipation region (Sironi et al. 2015). Needless to say, the magnetic reconnection scenario requires that jets carry a sizable fraction of their power in the magnetic form up to the emission regions.

Based on the jet parameters estimated in this paper, the magnetization properties can be studied. Here we define a magnetization parameter as the ratio of energy densities be-

¹¹If there is a dissipative mechanism, the magnetic energy could be converted to thermal and kinetic energy.

tween the magnetic field and relativistic electrons¹² $\sigma = U_B/U_e$ (also called the equipartition parameter). The distribution of σ is shown in the right panel of Figure 9. It can be seen that FSRQs have a narrower distribution than that of BL Lacs, with a median values $\sigma = 6.42$ and 0.0285 (and 0.640 for total blazars), respectively (see also Table 2). The Kolmogorov-Smirnov (KS) test yields the significance level probability for the null hypothesis that FSRQs and BL Lacs are drawn from the same distribution $p = 4.67 \times 10^{-76}$ and the statistic $D_{KS} = 0.503$ (the maximum separation of the two cumulative fractions). Similar results have been presented on single sources (Abdo et al. 2011; Acciari et al. 2011; Aleksić et al. 2015) and through modeling the SEDs of the large sample blazars (Zhang et al. 2013; Tavecchio & Ghisellini 2016), which demonstrate that the magnetization parameter of the large majority of BL Lacs is commonly at $\sim 10^{-2}$. Costamante et al. (2017) studied six hard-TeV BL Lacs and found that the equipartition parameters range from 10^{-3} to 10^{-5} . Kharb et al. (2012) presented a deep Chandra/ACIS observations and Hubble Space Telescope (HST) Advanced Camera for Surveys observations of two FSRQs, PKS B0106+013 and 3C 345, and found the shocked jet regions upstream of the radio hot spots, the kiloparsec-scale jet wiggles, and a “nose cone”-like jet structure in PKS B0106+013, as well as the V-shaped radio structure in 3C 345, which suggest that the jet still has a large σ at these large scale. Modelling of FSRQ SEDs is also in agreement with this result (e.g., Ghisellini & Tavecchio 2015).

The smaller σ in BL Lacs relative to FSRQs implies that BL Lacs jets would suffer deceleration more easily than those of FSRQs (Piner et al. 2008; Homan et al. 2015), although both present similar violent γ -ray emission from the central region. This is consistent with the idea that some BL Lacs show almost no superluminal motion in the Very Long Baseline Array (VLBA) scale (e.g., Mrk 501 and Mrk 421; Giroletti et al. 2004, 2006), while the multiwavelength SED and variability imply a highly Doppler-boosting emission, which indicates that the jet has already been decelerated at that scale (e.g., Ghisellini et al. 2005; Giroletti et al. 2004). For some FSRQs (e.g., 3C 279 and 3C 345; Piner et al. 2003; Lobanov & Zensus 1999), the Monitoring of Jets in AGN with VLBA Experiments (MOJAVE) project shows that jets will still be accelerated at the VLBA scale (see, Homan et al. 2015). The low magnetization in BL Lacs is essential in order to avoid efficient cooling of relativistic electrons, which would lead to much larger values of γ_0 of BL Lacs relative to FSRQs (see Table 2 and/or Figure 4). This also seems to imply that the magnetic reconnection cannot be strong in these emission regions. The particle acceleration in situ may originate from the energy dissipated in shocks and/or in boundary shear layers. The spine/layer jet

¹²Note that the definition of $\sigma = U_B/U_e$ here is different from $P_B/P_{\text{kin}} = U_B/(U_e + U_p)$. For typical jet parameters (median values), $U_p/U_e = 10^{3/4b}(m_p/m_e)/\gamma_0 \approx 28.0, 3.51, \text{ and } 11.6$ for FSRQs, BL Lacs, and total blazars.

structure has been revealed through many observational techniques and can contribute significant X-ray emission due to the enhancement of the seed photon energy density by relative opposite motions between the spine and layer (see Chen 2017, for recent review).

So far, there is no observational evidence supporting the theoretical prediction that a high-magnetization jet will more easily to transport energy to a large scale than a low-magnetization jet. As found above, FSRQs have relatively larger values of σ than BL Lacs, which simply predicts that the jet may transport energy more efficiently to a large scale in FSRQs than BL Lacs. Therefore, we may expect a larger extended jet kinetic power (relative to the core SED jet power) in FSRQs than BL Lacs. To answer this question, we should estimate the (extended) jet kinetic power of these sources.

The jet power is basically important for understanding jet formation, the jet-disk relation (Blandford & Znajek 1977; Blandford & Payne 1982; Gu et al. 2009; Spruit 2010; Narayan & McClintock 2012; Li & Cao 2012; Wu et al. 2013; Cao 2014), and the AGN feedback on structure formation (Magliocchetti & Brüggén 2007; Best et al. 2007). It is generally believed that the X-ray cavities are direct evidence of AGN feedback and provide a direct measurement of the mechanical energy released by the AGN jets (jet kinetic power) through the work done on the hot, gaseous halos surrounding them (e.g., Birzan et al. 2004; Allen et al. 2006; Cavagnolo et al. 2010). It is also found that the cavity kinetic power is correlated with the radio extended power (Rawlings & Saunders 1991; Birzan et al. 2004; Cavagnolo et al. 2010), and the scaling relationship is roughly consistent with the theoretical relation (e.g., Willott et al. 1999; Cavagnolo et al. 2010; Meyer et al. 2011). Therefore, in the systems where the X-ray cavities are lacking or not observed, the radio extended luminosity is used to estimate the jet kinetic power. The relations presented in Willott et al. (1999) are commonly used to do this estimation (Cavagnolo et al. 2010). Based on this method, Meyer et al. (2011) presented the largest blazar sample with measured (extended) jet kinetic power, until now.

In this paper, we collect the (extended) jet kinetic power, $P_{\text{jet,ext}}$, from Meyer et al. (2011), resulting in a total of 159 blazars, including 76 BL Lacs and 83 FSRQs, whose data are presented in Table 1. To study the jet energy transportation, we define η as a ratio of the jet SED power (from the central nuclei, P_{jet}) to the (extended) jet kinetic power ($P_{\text{jet,ext}}$), $\eta = P_{\text{jet}}/P_{\text{jet,ext}}$. The distribution of η is shown in Figure 10 with median values $\eta = 57.2$, 230, and 73.9 for FSRQs, BL Lacs, and total blazars, respectively, which implies that the jet SED power is significantly larger than the (extended) jet kinetic power. Two reasons may account for this: (1) the (SED) jet power may represent jet power measured in AGN active state, while the (extended) jet kinetic power is the historically average power, and 2) most of the energy is dissipated at the central region before being transported to a large scale. We

note that FSRQs have an average smaller η than BL Lacs (by about one order of magnitude). The KS test gives the significance level probability that FSRQs and BL Lacs are drawn from the same distribution $P = 2.58 \times 10^{-10}$ and the statistic $D_{\text{KS}} = 0.524$. This suggests that relatively more energy is transported to a large scale in FSRQs than in BL Lacs. As discussed above, the central jets of FSRQs also have relatively higher magnetization (σ) than those of BL Lacs, suggesting that a higher-magnetization jet can more easily transport energy to a large scale. As discussed above, some BL Lacs have extremely estimated Doppler factors. We instead use the median value of δ instead to determine the other jet parameters for these sources. This uncertainty may affect our results. Therefore, we exclude all BL Lacs with $\delta > 100$ or $\delta < 1$ and find that the remaining 56 BL Lacs have median values of $\eta = 230$ and $\sigma = 0.00389$, which is also consistent with the above result that the higher-magnetization jet can more easily transport energy to a large scale. For further research, we plot η versus σ in Figure 11 for sources with $1 < \delta < 100$, which presents a significant anticorrelation. The solid black line shows the best linear fit, $\log \sigma = (8.54 \pm 0.69) - (4.44 \pm 0.33) \log \eta$, with a chance probability $p = 1.23 \times 10^{-26}$ (Pearson test). This result confirms the above result, suggesting that a higher-magnetization jet can more easily transport energy to a larger scale, which, for the first time, offers supporting evidence for the jet energy transportation theory.

Our sample include 393 unknown-redshift sources (157 BL Lacs and 236 BCUs), which is about 28% of the sample. We use the median values of known redshifts of blazars for these sources. In order to explore the possible effect of this replacement on our results, we recalculate the median values of all jet parameters of another two cases: the case 1 uses known-redshift sources including BCUs, and the case 2 uses known-redshift sources excluding BCUs. All of these values are presented in the Table 2, where the label (z) is for the case 1 and the label (cz) is for the case 2. It can be seen that both cases are consistent with our above results.

5. Conclusion

In this paper, based on broadband SEDs, we estimate the jet physical parameters of 1392 γ -ray-loud AGNs (Ackermann et al. 2015; Fan et al. 2016). These values are presented in the Table 1, and the median values are shown in the Table 2, which are roughly consistent with previous studies. Out of these sources, the accretion disk luminosities of 232 sources and the (extended) kinetic jet powers of 159 sources are compiled from archived papers. The full version of the data is available online (publicly). The main results are summarized here.

1. We show that γ -ray FSRQs and BL Lacs are well separated by $\Gamma = -0.127 \log L_\gamma + 8.18$, in the γ -ray luminosity versus photon index plane with a success rate of 88.6%. This

criterion is employed to divide 311 BCUs into FSRQs or BL Lacs.

2. The peak electron energy γ_0 forms two distinct distributions between FSRQs and BL Lacs (also for ν_s/ν_C distributions), implying that the electrons in FSRQ jets suffer strong cooling, while they suffer less cooling in BL Lac jets.

3. A Significant number of FSRQs present a jet bolometric luminosity larger than disk luminosity by ~ 2 orders of magnitude, which implies a (SED) jet power (assuming typical values of the Doppler factor $\delta \sim 10$ and jet radiative efficiency $\sim 10\%$) larger than the disk luminosity by ~ 10 times. This suggests that the jet-launching processes and the way of transporting energy from the vicinity of the BH to infinity must be very efficient.

4. Most FSRQs present a (SED) jet power larger than the accretion power, which suggests that the relativistic jet-launching mechanism is dominated by the BZ process, at least in these FSRQs.

5. The magnetization of jets in BL Lacs is significantly lower than that in FSRQs, which is consistent with the idea that BL Lac jets may be more easily decelerated than FSRQ jets.

6. The ratio of the (extended) kinetic jet power to the (SED) jet power in FSRQs is significantly larger than that in BL Lacs. There is a significant anticorrelation between the jet magnetization parameter and the ratio of the SED jet power to the (extended) kinetic jet power. These results, for the first time, provide supporting evidence for the jet energy transportation theory: a high-magnetization jet can more easily transport energy to a large scale than a low-magnetization jet.

It should be noted that the nonsimultaneity of the SED does not always have an optimal impact on the derived parameters (and therefore large uncertainties) for single sources, but this is compensated for by the large number of sources ensuring that, from the statistical point of view, they should be only statistically meaningful.

We thank the anonymous referee for insightful comments and constructive suggestions. We are grateful for help from Xinwu Cao, Shiyin Shen, and Zhaoming Gan. This work is supported by the CAS grant (QYZDJ-SSW-SYS023).

REFERENCES

- Abdo, A. A., Ackermann, M., Agudo, I., et al. 2010, *ApJ*, 716, 30
- Abdo, A. A., Ackermann, M., Ajello, M., et al. 2010, *ApJ*, 715, 429
- Abdo, A. A., Ackermann, M., Ajello, M., et al. 2011, *ApJ*, 730, 101
- Abdo, A. A., Ackermann, M., Ajello, M., et al. 2009, *ApJ*, 700, 597
- Abdo, A. A., Ackermann, M., Ajello, M., et al. 2011, *ApJ*, 736, 131
- Acciari, V. A., Aliu, E., Arlen, T., et al. 2011, *ApJ*, 738, 25
- Acciari, V. A., Aliu, E., Aune, T., et al. 2009, *ApJ*, 707, 612
- Acerro, F., Ackermann, M., Ajello, M., et al. 2015, *ApJS*, 218, 23
- Ackermann, M., Ajello, M., Allafort, A., et al. 2011, *ApJ*, 743, 171
- Ackermann, M., Ajello, M., Atwood, W. B., et al. 2015, *ApJ*, 810, 14
- Aharonian, F. A. 2000, *New A*, 5, 377
- Aleksić, J., Ansoldi, S., Antonelli, L. A., et al. 2015, *MNRAS*, 451, 739
- Allen, S. W., Dunn, R. J. H., Fabian, A. C., et al. 2006, *MNRAS*, 372, 21
- Avara, M. J., McKinney, J. C., & Reynolds, C. S. 2016, *MNRAS*, 462, 636
- Birzan, L., Rafferty, D. A., McNamara, B. R., et al. 2004, *ApJ*, 607, 800
- Böttcher, M., & Chiang, J. 2002, *ApJ*, 581, 127
- Bai, J. M., Liu, H. T., & Ma, L. 2009, *ApJ*, 699, 2002
- Best, P. N., von der Linden, A., Kauffmann, G., et al. 2007, *MNRAS*, 379, 894
- Blandford, R. D., & Payne, D. G. 1982, *MNRAS*, 199, 883
- Blandford, R. D., & Rees, M. J. 1978, *BL Lac Objects*, 328
- Blandford, R. D., & Znajek, R. L. 1977, *MNRAS*, 179, 433
- Bloom, S. D., & Marscher, A. P. 1996, *ApJ*, 461, 657
- Blumenthal, G. R., & Gould, R. J. 1970, *Reviews of Modern Physics*, 42, 237

- Bonnoli, G., Ghisellini, G., Foschini, L., et al. 2011, MNRAS, 410, 368
- Calderone, G., Ghisellini, G., Colpi, M., & Dotti, M. 2013, MNRAS, 431, 210
- Cao, X. 2016, ApJ, 833, 30
- Cao, X. 2014, ApJ, 783, 51
- Cao, X. 2011, ApJ, 737, 94
- Cao, X. 2003, ApJ, 599, 147
- Cao, X. 2002, ApJ, 570, L13
- Cao, X., & Bai, J. M. 2008, ApJ, 673, L131
- Cao, X., & Jiang, D. R. 1999, MNRAS, 307, 802
- Cao, X., & Spruit, H. C. 2013, ApJ, 765, 149
- Cavagnolo, K. W., McNamara, B. R., Nulsen, P. E. J., et al. 2010, ApJ, 720, 1066
- Celotti, A., & Ghisellini, G. 2008, MNRAS, 385, 283
- Cerruti, M., Dermer, C. D., Lott, B., Boisson, C., & Zech, A. 2013, ApJ, 771, L4
- Cerutti, B., Werner, G. R., Uzdensky, D. A., & Begelman, M. C. 2012, ApJ, 754, L33
- Chen, L. 2017, ApJ, 842, 129
- Chen, L. 2014, ApJ, 788, 179
- Chen, L., & Bai, J. M. 2011, ApJ, 735, 108
- Chen, L., Cao, X., & Bai, J. M. 2012, ApJ, 748, 119
- Clausen-Brown, E., Savolainen, T., Pushkarev, A. B., et al. 2013, A&A, 558, A144
- Cleary, K., Lawrence, C. R., Marshall, J. A., Hao, L., & Meier, D. 2007, ApJ, 660, 117
- Costamante, L., Bonnoli, G., Tavecchio, F., et al. 2017, arXiv:1711.06282
- Dermer, C. D., Cerruti, M., Lott, B., Boisson, C., & Zech, A. 2014, ApJ, 782, 82
- Dermer, C. D., & Schlickeiser, R. 1993, ApJ, 416, 458
- Dermer, C. D., Yan, D., Zhang, L., Finke, J. D., & Lott, B. 2015, ApJ, 809, 174

- Ding, N., Zhang, X., Xiong, D. R., & Zhang, H. J. 2017, *MNRAS*, 464, 599
- Doeleman, S. S., Fish, V. L., Schenck, D. E., et al. 2012, *Science*, 338, 355
- Dondi, L., & Ghisellini, G. 1995, *MNRAS*, 273, 583
- Drenkhahn, G., & Spruit, H. C. 2002, *A&A*, 391, 1141
- Du, L. M., Xie, Z. H., Yi, T. F., et al. 2016, *New A*, 46, 9
- Falomo, R., Pian, E., & Treves, A. 2014, *A&A Rev.*, 22, 73
- Fan, J. H., Yang, J. H., Liu, Y., et al. 2016, *ApJS*, 226, 20
- Fan, J. H., Yang, J. H., Xiao, H. B., et al. 2017, *ApJ*, 835, L38
- Fan, J.-H., Bastieri, D., Yang, J.-H., et al. 2014, *RAA*, 14, 1135-1145
- Fan, J.-H., Huang, Y., He, T.-M., et al. 2009, *PASJ*, 61, 639
- Finke, J. D., Dermer, C. D., & Böttcher, M. 2008, *ApJ*, 686, 181-194
- Fossati, G., Maraschi, L., Celotti, A., et al. 1998, *MNRAS*, 299, 433
- Francis, P. J., Hewett, P. C., Foltz, C. B., et al. 1991, *ApJ*, 373, 465
- Ghisellini, G., Celotti, A., Fossati, G., et al. 1998, *MNRAS*, 301, 451
- Ghisellini, G., Maraschi, L., & Tavecchio, F. 2009, *MNRAS*, 396, L105
- Ghisellini, G., Padovani, P., Celotti, A., & Maraschi, L. 1993, *ApJ*, 407, 65
- Ghisellini, G., & Tavecchio, F. 2015, *MNRAS*, 448, 1060
- Ghisellini, G., & Tavecchio, F. 2010, *MNRAS*, 409, L79
- Ghisellini, G., & Tavecchio, F. 2009, *MNRAS*, 397, 985
- Ghisellini, G., Tavecchio, F., & Chiaberge, M. 2005, *A&A*, 432, 401
- Ghisellini, G., Tavecchio, F., Maraschi, L., et al. 2014, *Nature*, 515, 376
- Ghosh, P., & Abramowicz, M. A. 1997, *MNRAS*, 292, 887
- Giannios, D., Uzdensky, D. A., & Begelman, M. C. 2009, *MNRAS*, 395, L29
- Giroletti, M., Giovannini, G., Feretti, L., et al. 2004, *ApJ*, 600, 127

- Giroletti, M., Giovannini, G., Taylor, G. B., & Falomo, R. 2006, *ApJ*, 646, 801
- Giroletti, M., Giovannini, G., Taylor, G. B., & Falomo, R. 2004, *ApJ*, 613, 752
- Granot, J., Komissarov, S. S., & Spitkovsky, A. 2011, *MNRAS*, 411, 1323
- Greene, J. E., & Ho, L. C. 2005, *ApJ*, 630, 122
- Gu, M. 2013, *ApJ*, 773, 176
- Gu, M., Cao, X., & Jiang, D. R. 2009, *MNRAS*, 396, 984
- Gu, M., Cao, X., & Jiang, D. R. 2001, *MNRAS*, 327, 1111
- Hartman, R. C., Bertsch, D. L., Bloom, S. D., et al. 1999, *ApJS*, 123, 79
- Heinz, S., & Begelman, M. C. 2000, *ApJ*, 535, 104
- Ho, L. C., & Peng, C. Y. 2001, *ApJ*, 555, 650
- Homan, D. C., Lister, M. L., Kovalev, Y. Y., et al. 2015, *ApJ*, 798, 134
- Hoshino, M., Arons, J., Gallant, Y. A., & Langdon, A. B. 1992, *ApJ*, 390, 454
- Hovatta, T., Valtaoja, E., Tornikoski, M., & Lähteenmäki, A. 2009, *A&A*, 494, 527
- Hu, S. M., Chen, X., Guo, D. F., Jiang, Y. G., & Li, K. 2014, *MNRAS*, 443, 2940
- Hu, W., Dai, B.-Z., & Zeng, W. 2017, *arXiv:1711.05494*
- Janiak, M., Sikora, M., & Moderski, R. 2015, *MNRAS*, 449, 431
- Jorstad, S. G., Marscher, A. P., Lister, M. L., et al. 2005, *AJ*, 130, 1418
- Kang, S.-J., Chen, L., & Wu, Q. 2014, *ApJS*, 215, 5
- Katarzyński, K., Sol, H., & Kus, A. 2003, *A&A*, 410, 101
- Kaur, N., Chandra, S., Baliyan, K. S., Sameer, & Ganesh, S. 2017, *arXiv:1706.04411*
- Kellermann, K. I., Sramek, R., Schmidt, M., Shaffer, D. B., & Green, R. 1989, *AJ*, 98, 1195
- Kharb, P., Lister, M. L., Marshall, H. L., & Hogan, B. S. 2012, *ApJ*, 748, 81
- Kirk, J. G., Rieger, F. M., & Mastichiadis, A. 1998, *A&A*, 333, 452
- Komissarov, S. S. 2011, *Mem. Soc. Astron. Italiana*, 82, 95

- Komissarov, S. S., Barkov, M. V., Vlahakis, N., & Königl, A. 2007, MNRAS, 380, 51
- Komissarov, S. S., Vlahakis, N., Königl, A., & Barkov, M. V. 2009, MNRAS, 394, 1182
- Krauß, F., Wilms, J., Kadler, M., et al. 2016, A&A, 591, A130
- Lähteenmäki, A., & Valtaoja, E. 1999, ApJ, 521, 493
- Laor, A. 2001, ApJ, 553, 677
- Li, S.-L. 2014, ApJ, 788, 71
- Li, S.-L., & Cao, X. 2012, ApJ, 753, 24
- Li, Z.-Y., Chiueh, T., & Begelman, M. C. 1992, ApJ, 394, 459
- Liao, N. H., Bai, J. M., Liu, H. T., et al. 2014, ApJ, 783, 83
- Liodakis, I., Marchili, N., Angelakis, E., et al. 2017, MNRAS, 466, 4625
- Lister, M. L., Aller, M. F., Aller, H. D., et al. 2013, AJ, 146, 120
- Liu, H. T., & Bai, J. M. 2006, ApJ, 653, 1089
- Liu, H. T., Bai, J. M., Wang, J. M., & Li, S. K. 2014, AJ, 147, 17
- Livio, M., Ogilvie, G. I., & Pringle, J. E. 1999, ApJ, 512, 100
- Lobanov, A. P., & Zensus, J. A. 1999, ApJ, 521, 509
- Lovelace, R. V. E., Wang, J. C. L., & Sulkanen, M. E. 1987, ApJ, 315, 504
- Lyubarsky, Y. E. 2010, MNRAS, 402, 353
- Lyubarsky, Y. 2010, ApJ, 725, L234
- Lyutikov, M., & Lister, M. 2010, ApJ, 722, 197
- Ma, R., Xie, F.-G., & Hou, S. 2014, ApJ, 780, L14
- Madejski, G. (., & Sikora, M. 2016, ARA&A, 54, 725
- Magliocchetti, M., & Brüggén, M. 2007, MNRAS, 379, 260
- Mannheim, K. 1993, A&A, 269, 67
- Marscher, A. P. 2014, ApJ, 780, 87

- Massaro, E., Perri, M., Giommi, P., & Nesci, R. 2004, *A&A*, 413, 489
- Massaro, E., Tramacere, A., Perri, M., Giommi, P., & Tosti, G. 2006, *A&A*, 448, 861
- Mattox, J. R., Bertsch, D. L., Chiang, J., et al. 1993, *ApJ*, 410, 609
- McKinney, J. C., Tchekhovskoy, A., & Blandford, R. D. 2012, *MNRAS*, 423, 3083
- Meier, D. L. 2002, *New A Rev.*, 46, 247
- Meyer, E. T., Fossati, G., Georganopoulos, M., & Lister, M. L. 2011, *ApJ*, 740, 98
- Michel, F. C. 1969, *ApJ*, 158, 727
- Moderski, R., Sikora, M., & Błażejowski, M. 2003, *A&A*, 406, 855
- Nalewajko, K. 2013, *MNRAS*, 430, 1324
- Nalewajko, K., Begelman, M. C., & Sikora, M. 2014, *ApJ*, 789, 161
- Nalewajko, K., Sikora, M., & Begelman, M. C. 2014, *ApJ*, 796, L5
- Nandikotkur, G., Jahoda, K. M., Hartman, R. C., et al. 2007, *ApJ*, 657, 706
- Narayan, R., Igumenshchev, I. V., & Abramowicz, M. A. 2003, *PASJ*, 55, L69
- Narayan, R., & McClintock, J. E. 2012, *MNRAS*, 419, L69
- Nemmen, R. S., Georganopoulos, M., Guiriec, S., et al. 2012, *Science*, 338, 1445
- Nieppola, E., Valtaoja, E., Tornikoski, M., et al. 2008, *A&A*, 488, 867
- Piner, B. G., Pant, N., & Edwards, P. G. 2008, *ApJ*, 678, 64-77
- Piner, B. G., Unwin, S. C., Wehrle, A. E., et al. 2003, *ApJ*, 588, 716
- Planck Collaboration, Ade, P. A. R., Aghanim, N., et al. 2014, *A&A*, 571, A16
- Pushkarev, A. B., Kovalev, Y. Y., Lister, M. L., & Savolainen, T. 2009, *A&A*, 507, L33
- Qin, L., Wang, J., Yang, C., et al. 2018, *arXiv:1711.10625*
- Rawlings, S., & Saunders, R. 1991, *Nature*, 349, 138
- Rees, M. J. 1984, *ARA&A*, 22, 471
- Richards, G. T., Lacy, M., Storrie-Lombardi, L. J., et al. 2006, *ApJS*, 166, 470

- Rybicki, G. B., & Lightman, A. P. 1979, New York, Wiley-Interscience, 1979. 393 p.,
- Savolainen, T., Homan, D. C., Hovatta, T., et al. 2010, *A&A*, 512, A24
- Sbarrato, T., Ghisellini, G., Tagliaferri, G., et al. 2016, *MNRAS*, 462, 1542
- Sbarrato, T., Padovani, P., & Ghisellini, G. 2014, *MNRAS*, 445, 81
- Scarpa, R., & Falomo, R. 1997, *A&A*, 325, 109
- Shakura, N. I., & Sunyaev, R. A. 1973, *A&A*, 24, 337
- Shaw, M. S., Romani, R. W., Cotter, G., et al. 2012, *ApJ*, 748, 49
- Shen, Y., Richards, G. T., Strauss, M. A., et al. 2011, *ApJS*, 194, 45
- Sikora, M. 2016, *Galaxies*, 4, 12
- Sikora, M., & Begelman, M. C. 2013, *ApJ*, 764, L24
- Sikora, M., Begelman, M. C., & Rees, M. J. 1994, *ApJ*, 421, 153
- Sikora, M., Stawarz, L., Moderski, R., Nalewajko, K., & Madejski, G. M. 2009, *ApJ*, 704, 38
- Sironi, L., Petropoulou, M., & Giannios, D. 2015, *MNRAS*, 450, 183
- Sironi, L., & Spitkovsky, A. 2011, *ApJ*, 726, 75
- Spruit, H. C. 2010, *Lecture Notes in Physics*, Berlin Springer Verlag, 794, 233
- Spruit, H. C., Daigne, F., & Drenkhahn, G. 2001, *A&A*, 369, 694
- Swanenburg, B. N., Bennett, K., Bignami, G. F., et al. 1978, *Nature*, 275, 298
- Tavecchio, F., & Ghisellini, G. 2016, *MNRAS*, 456, 2374
- Tavecchio, F., Ghisellini, G., Ghirlanda, G., et al. 2010, *MNRAS*, 401, 1570
- Tavecchio, F., Pacciani, L., Donnarumma, I., et al. 2013, *MNRAS*, 435, L24
- Tavecchio, F., Maraschi, L., & Ghisellini, G. 1998, *ApJ*, 509, 608
- Tavecchio, F., & Mazin, D. 2009, *MNRAS*, 392, L40
- Tchekhovskoy, A., McKinney, J. C., & Narayan, R. 2009, *ApJ*, 699, 1789
- Tchekhovskoy, A., Narayan, R., & McKinney, J. C. 2011, *MNRAS*, 418, L79

- Thorne, K. S. 1974, *ApJ*, 191, 507
- Tramacere, A., Massaro, E., & Taylor, A. M. 2011, *ApJ*, 739, 66
- Ulrich, M.-H., Maraschi, L., & Urry, C. M. 1997, *ARA&A*, 35, 445
- Urry, C. M., & Padovani, P. 1995, *PASP*, 107, 803
- Uzdensky, D. A. 2011, *Space Sci. Rev.*, 160, 45
- Vanden Berk, D. E., Richards, G. T., Bauer, A., et al. 2001, *AJ*, 122, 549
- Vestergaard, M., & Peterson, B. M. 2006, *ApJ*, 641, 689
- Vlahakis, N. 2015, *The Formation and Disruption of Black Hole Jets*, 414, 177
- Vlahakis, N., & Königl, A. 2004, *ApJ*, 605, 656
- Vlahakis, N., & Königl, A. 2001, *ApJ*, 563, L129
- Wang, J.-M., Ho, L. C., & Staubert, R. 2003, *A&A*, 409, 887
- Wang, J.-M., Staubert, R., & Ho, L. C. 2002, *ApJ*, 579, 554
- Weber, E. J., & Davis, L., Jr. 1967, *ApJ*, 148, 217
- Willott, C. J., Rawlings, S., Blundell, K. M., & Lacy, M. 1999, *MNRAS*, 309, 1017
- Wu, Q., Cao, X., Ho, L. C., & Wang, D.-X. 2013, *ApJ*, 770, 31
- Wu, X.-B., Wang, R., Kong, M. Z., Liu, F. K., & Han, J. L. 2004, *A&A*, 424, 793
- Wu, X.-B., Liu, F. K., & Zhang, T. Z. 2002, *A&A*, 389, 742
- Wu, Z.-Z., Gu, M.-F., & Jiang, D.-R. 2009, *Research in Astronomy and Astrophysics*, 9, 168
- Xiong, D. R., & Zhang, X. 2014, *MNRAS*, 441, 3375
- Xu, Y.-D., Cao, X., & Wu, Q. 2009, *ApJ*, 694, L107
- Xue, R., Luo, D., Du, L. M., et al. 2016, *MNRAS*, 463, 3038
- Yan, D., Zhang, L., & Zhang, S.-N. 2015, *MNRAS*, 454, 1310
- Yuan, F., & Narayan, R. 2014, *ARA&A*, 52, 529
- Yuan, W., Zhou, H. Y., Komossa, S., et al. 2008, *ApJ*, 685, 801-827

- Zamaninasab, M., Clausen-Brown, E., Savolainen, T., et al. 2014, *Nature*, 510, 126
- Zdziarski, A. A., Sikora, M., Pjanka, P., & Tchekhovskoy, A. 2015, *MNRAS*, 451, 927
- Zhang, J., Liang, E.-W., Sun, X.-N., et al. 2013, *ApJ*, 774, L5
- Zhang, J., Liang, E.-W., Zhang, S.-N., & Bai, J. M. 2012, *ApJ*, 752, 157
- Zhang, J., Xue, Z.-W., He, J.-J., Liang, E.-W., & Zhang, S.-N. 2015, *ApJ*, 807, 51

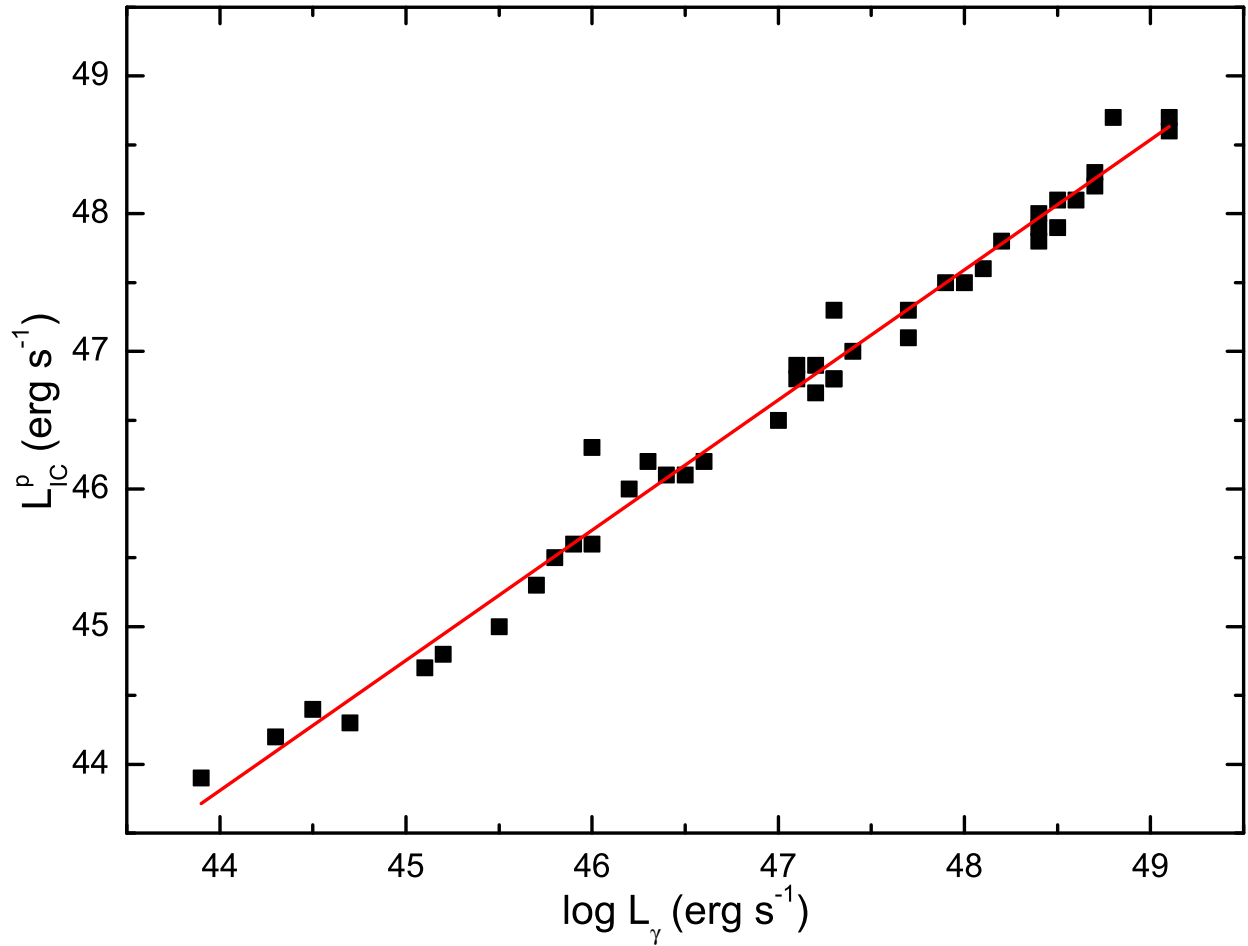


Fig. 1.— Relation between γ -ray luminosity and IC peak luminosity for blazars from Abdo et al. (2010), with the best linear fit $\log L_{IC}^p = (0.946 \pm 0.018) \log L_\gamma + (2.18 \pm 0.88)$ and the chance probability $p = 8.72 \times 10^{-39}$ (Pearson test).

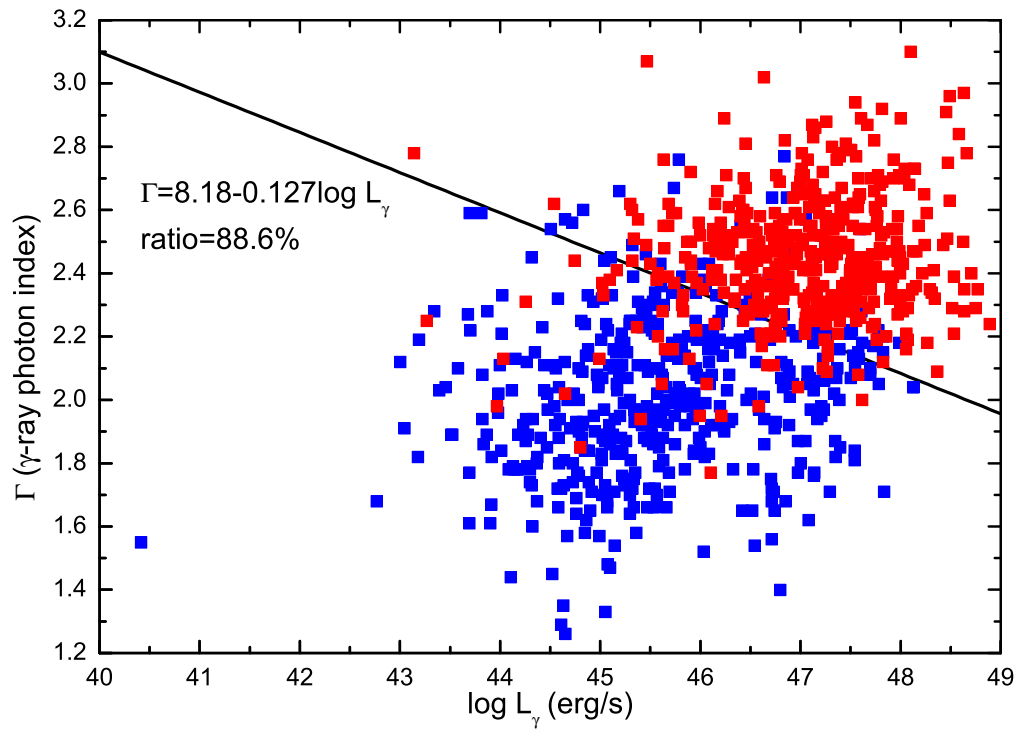


Fig. 2.— The γ -ray photon index versus γ -ray luminosity. The FSRQs and BL Lacs are well separated by $\Gamma = -0.127 \log L_\gamma + 8.18$, with a success rate of 88.6%.

Table 1: AGN Jet physical parameters

Name	z	Cl.	$\log \gamma_0$	b	$\log R$	δ	$\log B$	$\log P_{\text{jet}}$	$\log \sigma$	$\log \eta$	$\log M$	$\log L_{\text{disk}}$	Model
(1)	(2)	(3)	(4)	(5)	(6)	(7)	(8)	(9)	(10)	(11)	(12)	(13)	(14)
J0001.2-0748	-	CB	4.25	0.60	17.2	56.1	-2.46	46.6	-3.36	-	-	-	ST

.....

Note. The source names labeled with “*” are blazars having extreme Doppler factors ($\delta < 1$ or $\delta > 100$), and therefore we instead use the median values ($\delta_{\text{m}} \simeq 14.3$ for BL Lacs and $\delta_{\text{m}} \simeq 10.7$ for FSRQs) instead to calculate other jet parameters (see text for details). Column (1) gives the 3FGL name. Column (2) gives the redshift. Column (3) is the class of the source: “UF” for BCUs classified as FSRQs, “UB” for BCUs classified as BL Lacs, and “CF” and “CB” for confirmed FSRQs and BL Lacs, respectively. Column (4) is the electron peak energy. Column (5) is the curvature b of the electron energy distribution. Column (6) is the radius of the emission sphere in units of cm. Column (7) is the Doppler factor. Column (8) is the strength of the magnetic field in units of Gs. Column (9) is the jet (SED) power in units of erg s^{-1} . Column (10) is the magnetization parameter $\sigma = U_{\text{B}}/U_{\text{e}}$. Column (11) is the ratio of the jet SED power to (extended) jet kinetic power, $\eta = P_{\text{jet}}/P_{\text{jet,ext}}$. Column (12) is the available BH mass in units of M_{\odot} . Column (13) is the available disk luminosity in units of erg s^{-1} . Column (14) is the model used in the calculations: “ST” for SSC/Thomson, “SK” for SSC/KN, “ET” for EC/Thomson, and “EK” for EC/KN.

(This table is available in its entirety in ASCII text form.)

Table 2: Median values of Some jet physical parameters

	γ_0	b	R	δ	B	P_{jet}	η	σ	$P_{\text{jet}}/L_{\text{acc}}$	$P_{\text{jet}}/L_{\text{Edd}}$	$L_{\text{disk}}/L_{\text{Edd}}$
	(1)	(2)	(3)	(4)	(5)	(6)	(7)	(8)	(9)	(10)	(11)
FSRQ(t)	1167.8	0.6	2.78	10.7	1.56	20.0	57.2	6.42	0.768	0.382	0.148
BL Lac(t)	12077	0.55	3.70	14.3	0.119	6.3	230	0.0285	-	-	-
Total(t)	3646.1	0.55	3.70	14.3	0.446	12.0	73.9	0.640	-	-	-
FSRQ(z)	1075.9	0.65	2.93	11.3	1.54	22.2	57.2	6.42	0.768	0.382	0.148
BL Lac(z)	13888	0.55	3.70	14.3	0.0748	5.08	230	0.0121	-	-	-
Total(z)	2713.3	0.60	3.70	14.3	0.528	14.8	73.9	0.743	-	-	-
FSRQ(cz)	1050.8	0.65	2.96	11.4	1.54	22.2	57.2	6.43	0.768	0.382	0.148
BL Lac(cz)	14036	0.55	3.70	14.3	0.0768	5.11	213	0.0131	-	-	-
Total(cz)	2614.6	0.60	3.70	14.3	0.554	15.3	73.4	0.862	-	-	-

Note. Case (t) is for all sources in our sample. Case (z) is for sources having known redshifts and including BCUs, while case (cz) is for sources having known redshifts and excluding BCUs. Column (1) is the electron peak energy. Column (2) is the curvature of the electron energy distribution. Column (3) is the radius of the emission sphere in units of 10^{16} cm. Column (4) is the Doppler factor. Column (5) is the strength of the magnetic field in units of Gs. Column (6) is the jet (SED) power in units of 10^{45} erg s^{-1} . Column (7) is the ratio of the jet SED power to the (extended) jet kinetic power, $\eta = P_{\text{jet}}/P_{\text{jet,ext}}$. Column (8) is the magnetization parameter $\sigma = U_{\text{B}}/U_{\text{e}}$. Column (9) is the jet power in units of accretion power. Column (10) is the jet power in unit of Eddington power. Column (11) is the disk luminosity in units of Eddington power.

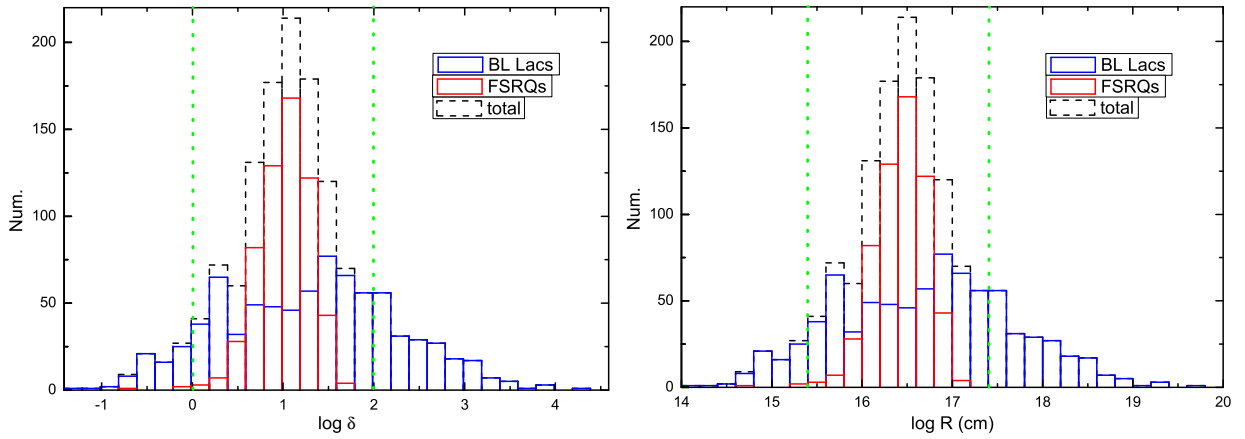


Fig. 3.— Distributions of δ and R . Left panel: The median values of the Doppler factor δ of FSRQs, BL Lacs, and total blazars are 10.7, 22.4, and 13.1, respectively. For sources with $1 < \delta < 100$ (i.e., within the two green dotted lines), the median values of δ of FSRQs and BL Lacs are 10.7 and 14.3, respectively. Right panel: The median values of the size of the emission region R of FSRQs, BL Lacs, and total blazars are 2.76 , 5.79 , and 3.38×10^{16} cm, respectively. For sources with $1 < \delta < 100$ (i.e., within the two green dotted lines), the median values of R of FSRQs and BL Lacs are 2.78 and 3.70×10^{16} cm, respectively. See also the Table 2.

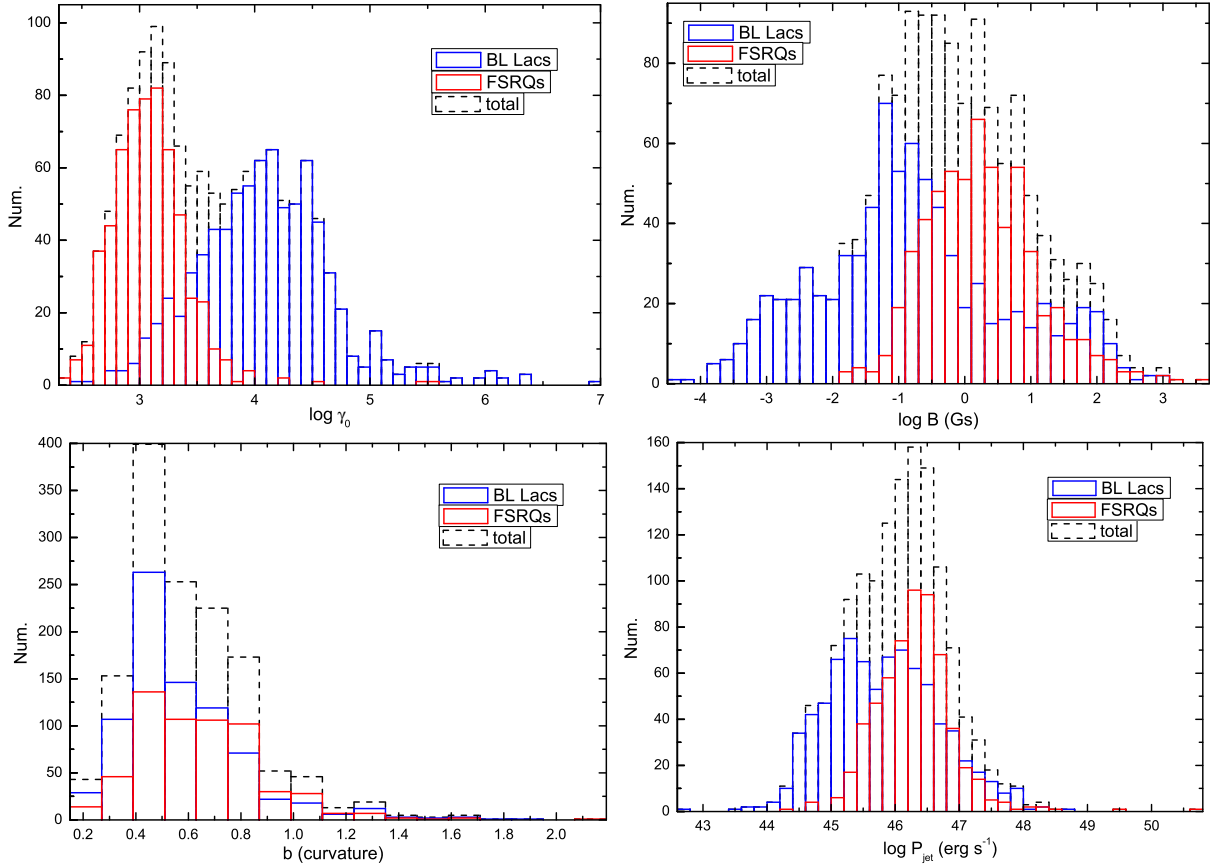


Fig. 4.— Distributions of some jet parameters. Upper left panel: The median values of the electron peak energy γ_0 of FSRQs, BL Lacs, and total blazars are 1167.8, 12077, and 3646.1, respectively. Upper right panel: The median values of the strength of the magnetic field B of FSRQs, BL Lacs, and total blazars are 1.56, 0.119, and 0.446, respectively. Bottom left panel: The median values of the curvature b of FSRQs, BL Lacs, and total blazars are 0.6, 0.55, and 0.55, respectively. Bottom right panel: The median values of the jet power P_{jet} of FSRQs, BL Lacs, and total blazars are 20.0, 6.3, and 12.0×10^{45} erg s⁻¹, respectively. See also the Table 2.

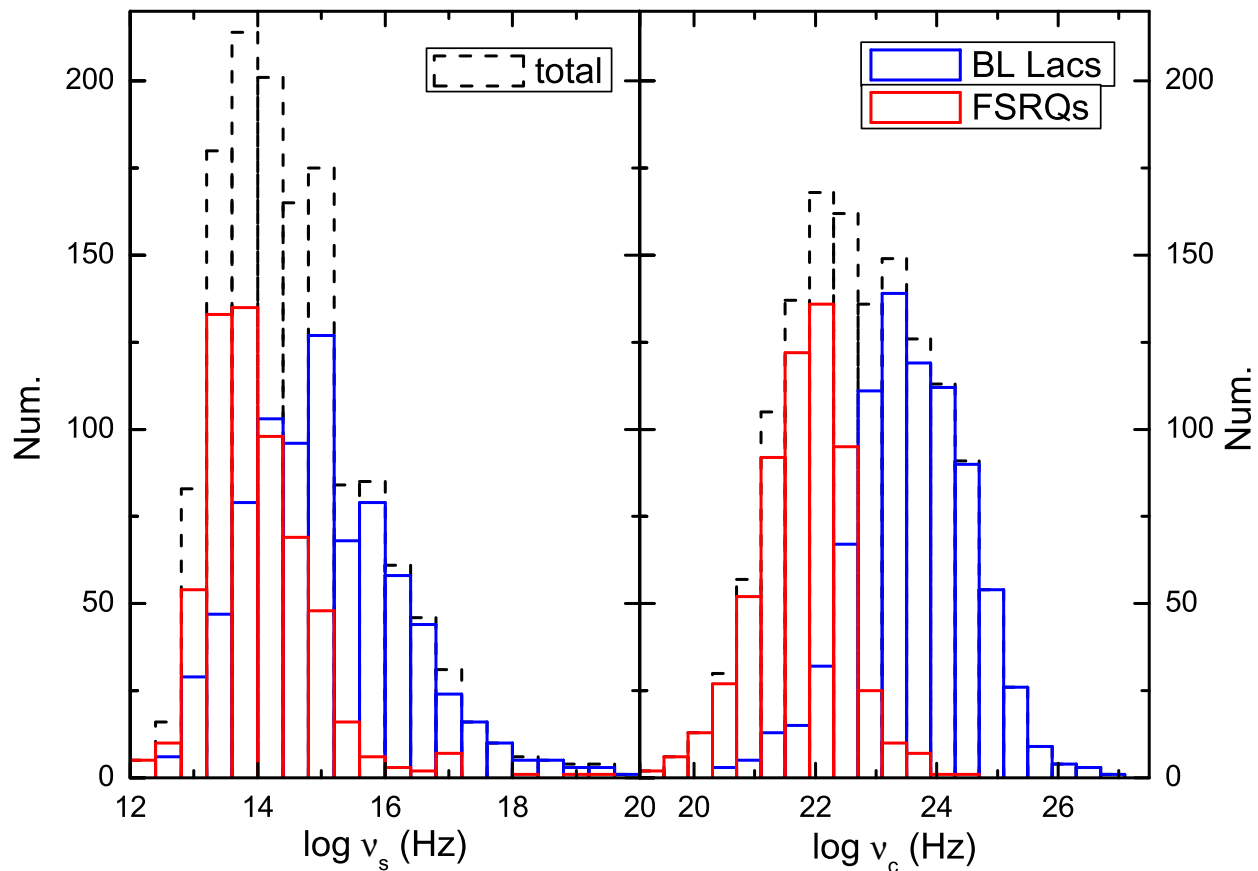


Fig. 5.— Distribution of synchrotron (left panel) and IC (right panel) peak frequency (measured in the AGN frame). The median values are $\nu_s = (0.689, 8.13, 2.48) \times 10^{14}$ Hz and $\nu_c = (0.692, 33.1, 5.75) \times 10^{22}$ Hz for FSRQs, BL Lacs, and total blazars, respectively.

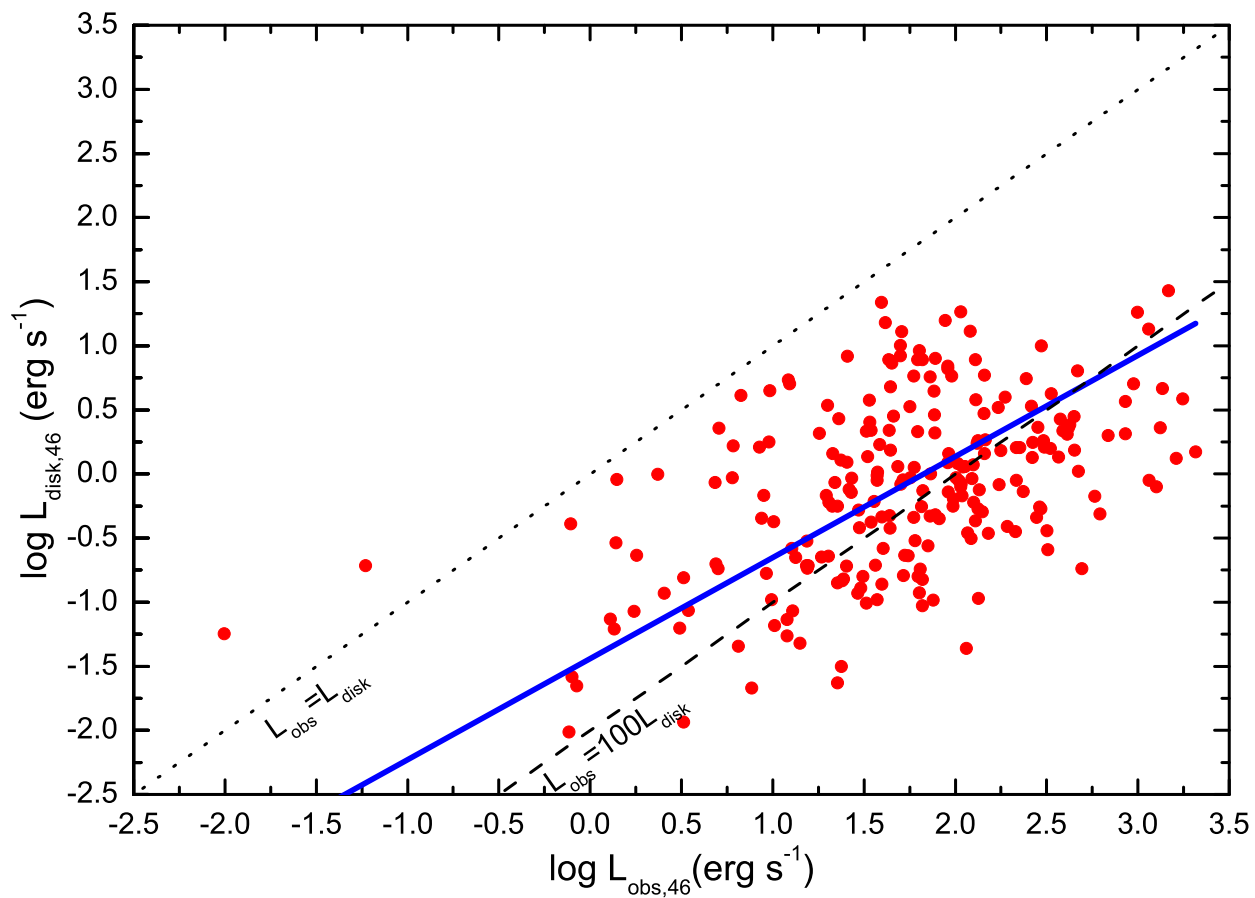


Fig. 6.— Jet bolometric luminosity versus disk luminosity. The solid blue line shows a robust correlation, $\log L_{\text{disk},46} = (0.788 \pm 0.076) \log L_{\text{obs},46} - (1.44 \pm 0.14)$, with a chance probability $p = 4.76 \times 10^{-15}$ through a Pearson test. The black dotted line represents $L_{\text{obs}} = L_{\text{disk}}$ and the black dashed line $L_{\text{obs}} = 100 L_{\text{disk}}$.

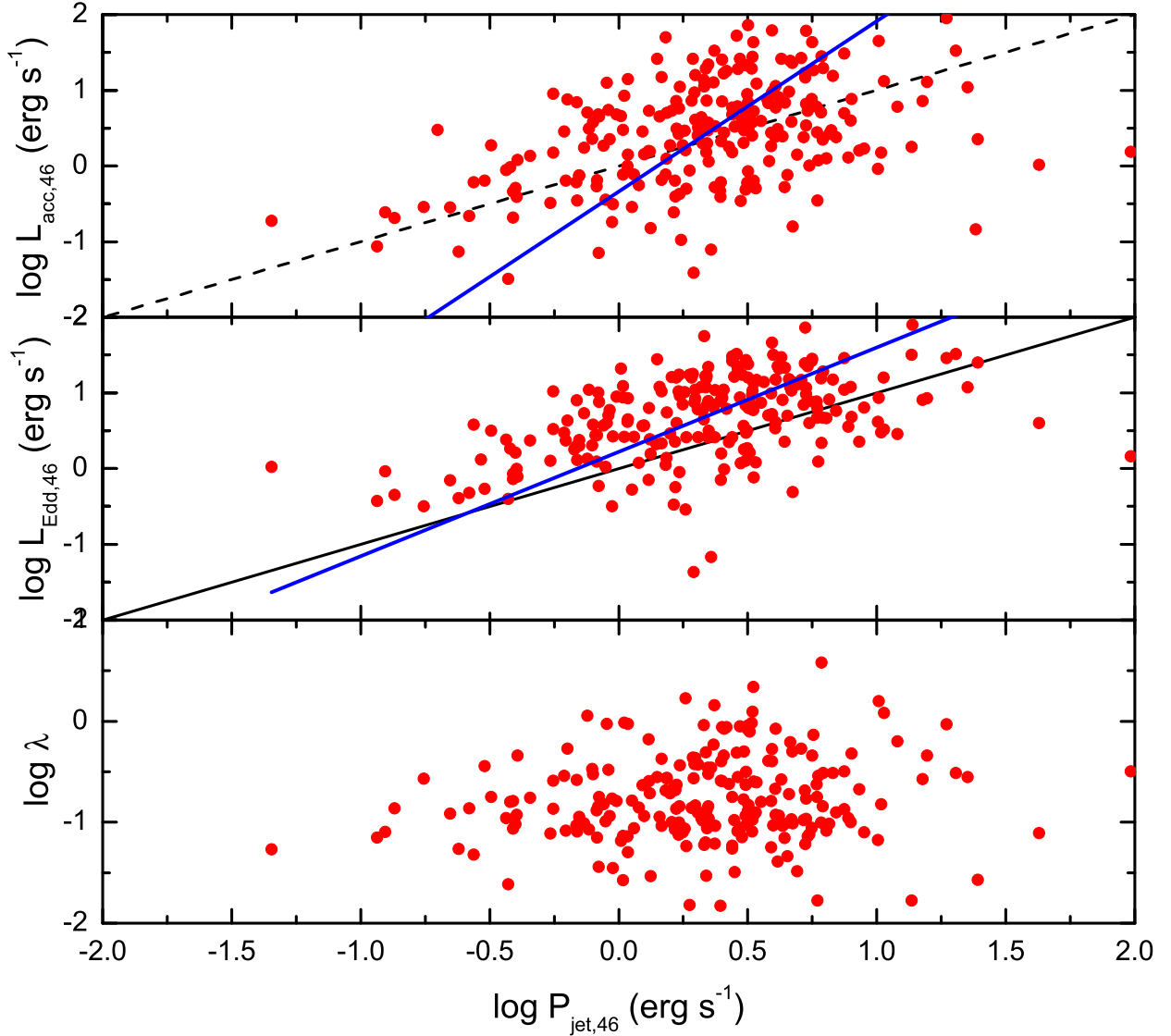


Fig. 7.— Jet power P_{jet} versus the accretion power L_{acc} (upper panel), Eddington luminosity L_{Edd} (middle panel), and Eddington ratio λ (bottom panel). The solid blue lines show robust correlations, $\log L_{\text{acc},46} = (2.25 \pm 0.27) \log P_{\text{jet},46} - (0.34 \pm 0.12)$, with a chance probability $p = 2.76 \times 10^{-11}$ (Pearson test) for upper panel and $\log L_{\text{Edd},46} = (1.38 \pm 0.14) \log P_{\text{jet},46} + (0.215 \pm 0.064)$, with a chance probability $p = 2.98 \times 10^{-14}$ (Pearson test) for the middle panel. The black dashed line is an equality line. There is almost no correlation between the jet power and Eddington ratio (chance probability $p = 0.0354$).

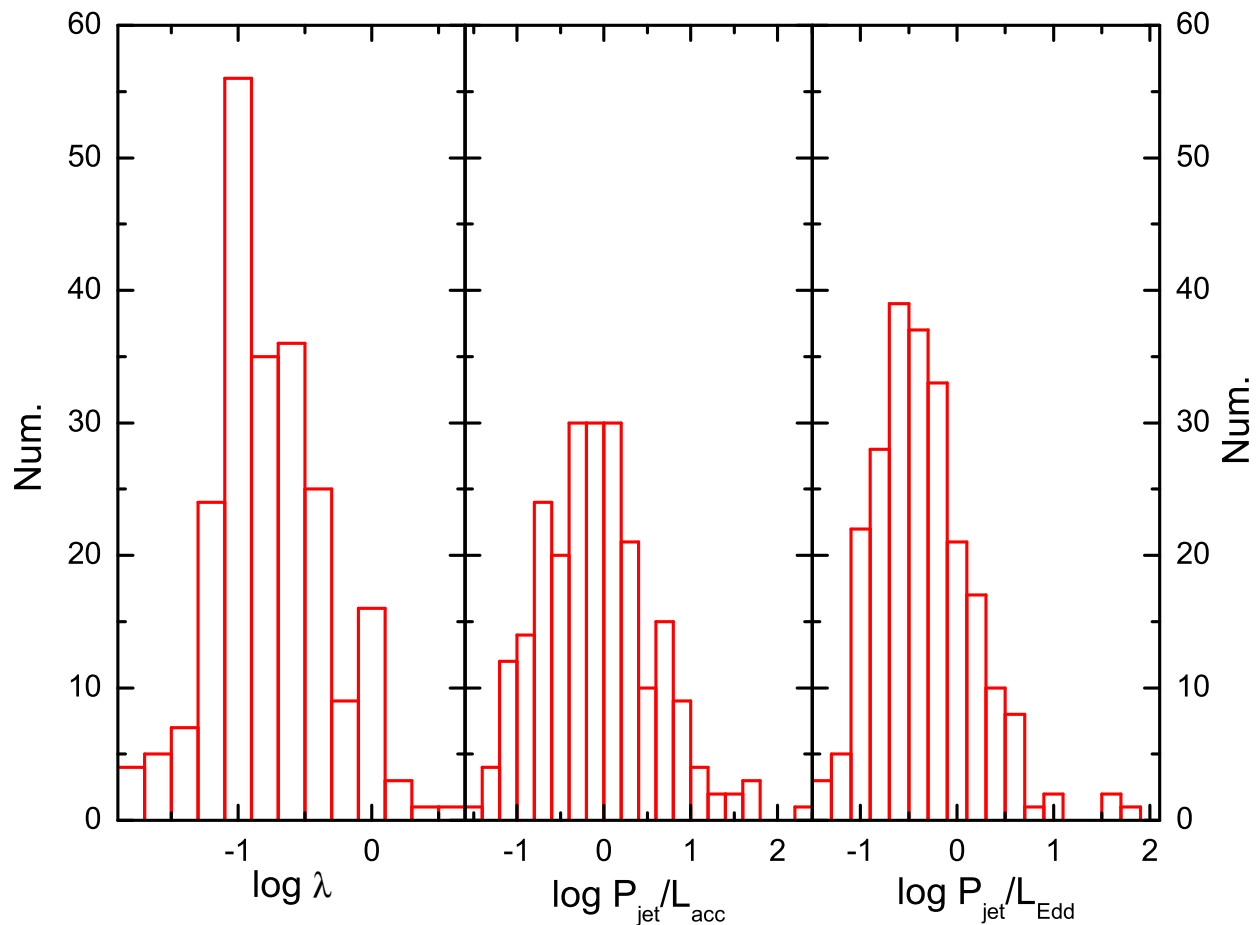


Fig. 8.— Distributions of Eddington ratio (left panel) and the jet power in units of accretion power ($P_{\text{jet}}/P_{\text{acc}}$, middle panel) and Eddington power ($P_{\text{jet}}/L_{\text{Edd}}$, right panel), of which the median values are 0.148, 0.768, and 0.382, respectively.

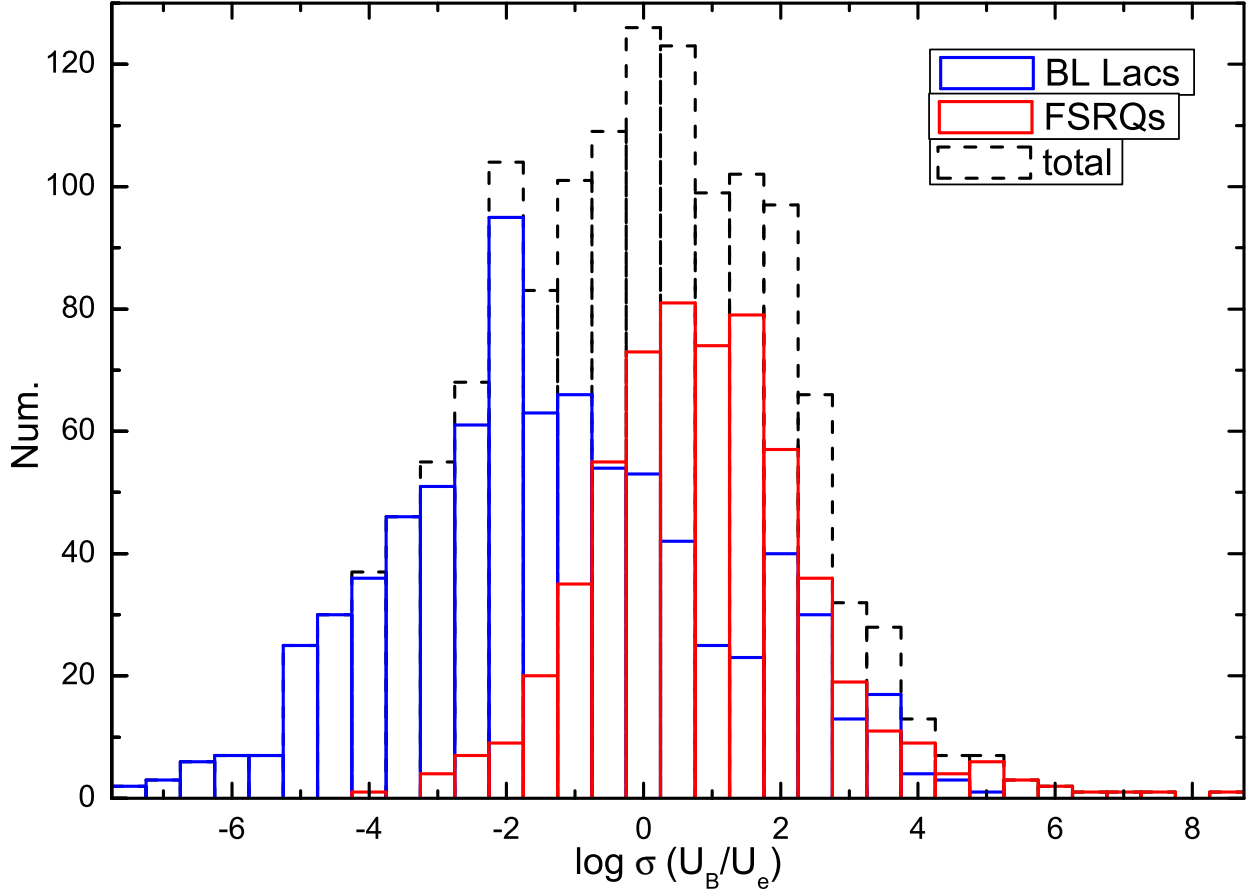


Fig. 9.— Distribution of the magnetization parameters $\sigma = U_B/U_e$ of a total of 1392 blazars with median values of FSRQs, BL Lacs, and total blazars of 6.42, 0.0285, and 0.640, respectively. The KS test yields the significance level probability for the null hypothesis that FSRQs and BL Lacs are drawn from the same distribution $P = 4.67 \times 10^{-76}$ and the statistic $D_{KS} = 0.503$ (the maximum separation of the two cumulative fractions).

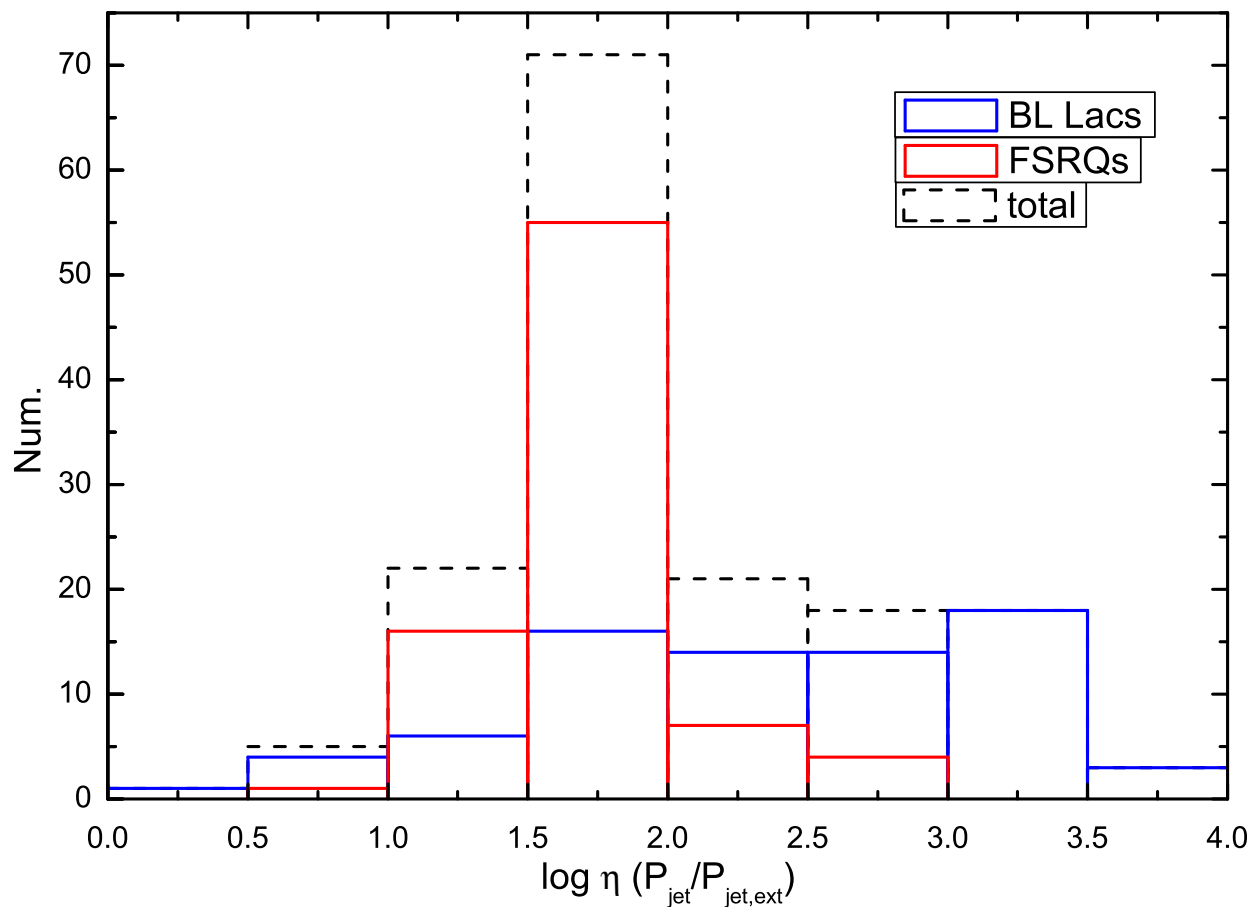


Fig. 10.— Distribution of $\eta = P_{\text{jet}}/P_{\text{jet,ext}}$ for blazars having measured extended radio emission (159 blazars, including 83 FSRQs and 76 BL Lacs), with median values of 57.2, 230, and 73.9 for FSRQs, BL Lacs, and total blazars, respectively. The KS test gives the significance level probability that FSRQs and BL Lacs are drawn from the same distribution $P = 2.58 \times 10^{-10}$ and the statistic $D_{\text{KS}} = 0.524$.

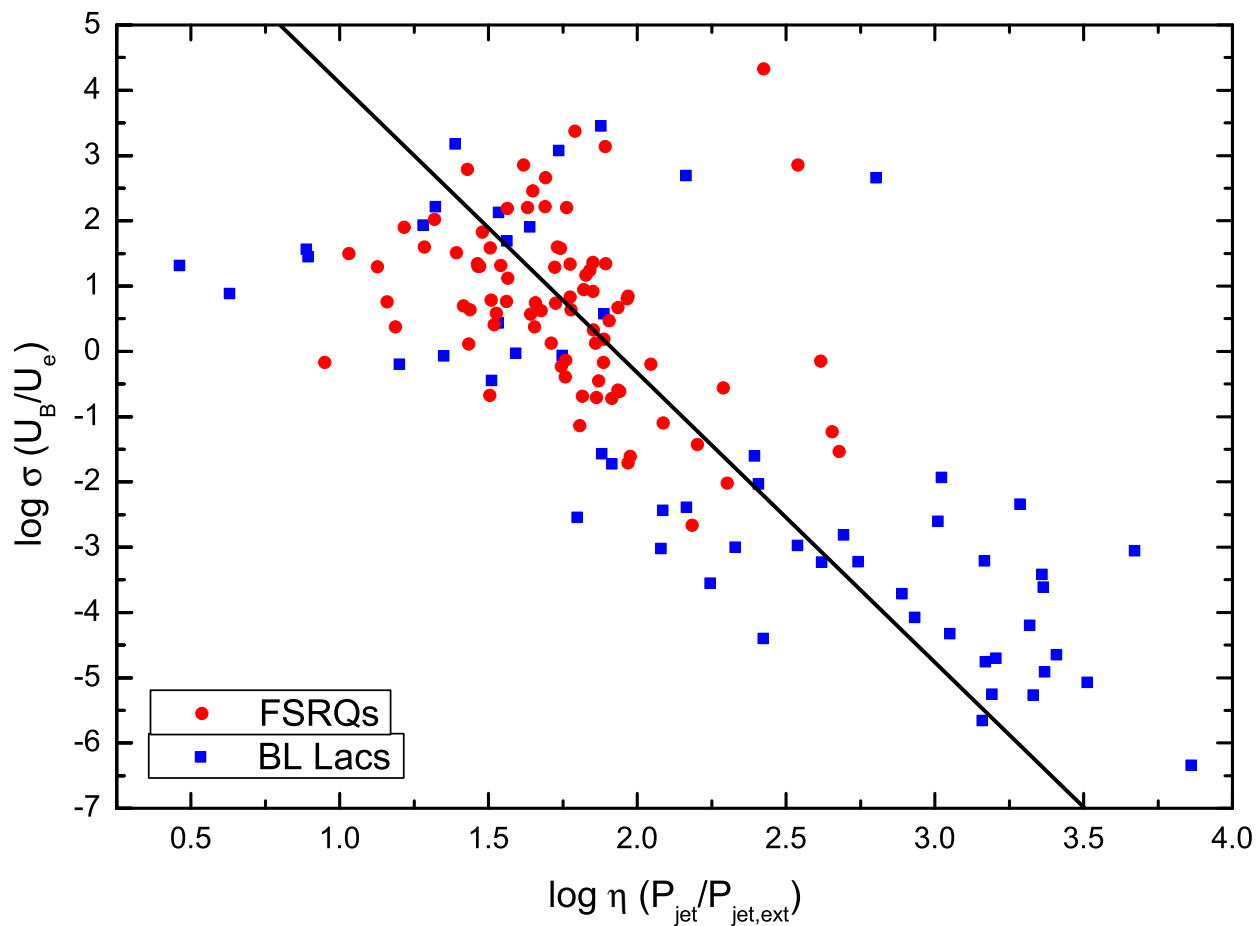


Fig. 11.— Jet magnetization parameters ($\sigma = U_B/U_e$) versus the ratio of (SED) jet power to (extended) kinetic jet power ($\eta = P_{\text{jet}}/P_{\text{jet,ext}}$). The solid black line presents a best linear fit for the total sources, $\log \sigma = -(4.44 \pm 0.33) \log \eta + (8.54 \pm 0.69)$, with a chance probability $p = 1.23 \times 10^{-26}$ (Pearson test).